Macromolecules

pubs.acs.org/Macromolecules Article

Bottom-up Construction of Dynamic Density Functional Theories for Inhomogeneous Polymer Systems from Microscopic Simulations

Sriteja Mantha, Shuanhu Qi, and Friederike Schmid*

Cite This: *Macromolecules* 2020, 53, 3409−3423 Read Online

ACCESS | Metrics & More | Article Recommendations

ABSTRACT: We propose and compare different strategies to construct dynamic density functional theories (DDFTs) for inhomogeneous polymer systems close to equilibrium from microscopic simulation trajectories. We focus on the systematic construction of the mobility coefficient, $\Lambda(\mathbf{r},\mathbf{r}')$, which relates the thermodynamic driving force on monomers at position $\mathbf{r}'$ to the motion of monomers at position $\mathbf{r}$. A first approach based on the Green−Kubo formalism turns out to be impractical because of a severe plateau problem. Instead, we propose to extract the mobility coefficient from an effective characteristic relaxation time of the single chain dynamic structure factor. To test our approach, we study the kinetics of ordering and disordering in diblock copolymer melts. The DDFT results are in very good agreement with the data from corresponding fine-grained simulations.

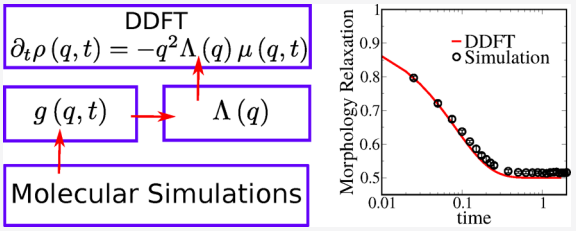

1. INTRODUCTION

Inhomogeneous polymer systems assemble into ordered morphologies due to incompatible interactions between different constituents in the systems.[1,2] These assembled morphologies have found applications as thermoplastic elastomers,[3] materials for drug delivery and release,[4] gas capture,[5] water purification,[6] energy conversion,[7,8] and also in soft lithography.[9] Understanding the relation between the molecular features of polymers and the ordered morphologies formed by them has been a subject of active investigation for a long time.[10−13] An equally interesting topic is the effect of polymer dynamics on the process of self-assembly,[14] for example, on the kinetics of defect formation depending on the way a nanostructured polymer material is processed.[15−19] This has led to experimental and theoretical investigations to understand the polymer dynamics in inhomogeneous systems and its effect on the formation of ordered morphologies.

Different scattering and reflectometry techniques have been employed to study the kinetic pathways leading to order−order and order−disorder transitions in block copolymer systems.[20−27] The same techniques are used to investigate the adsorption dynamics and the formation of interfaces in an incompatible homopolymer blend.[28−37] However, the dynamics in inhomogeneous polymer systems involves relaxation processes occurring over multiple length and time scales. For example, the molecular features of polymers determine the local rearrangements of chains. On the other hand, the mesoscopic ordering of polymer chains takes place on length and time scales which are multiple orders of magnitude higher than the molecular length and time scales. As a result, finding an experimental technique that can capture the dynamics over the entire spectrum of length and time scales is an extremely involved task. Dynamic density functional theory (DDFT)[38−43] or the dynamic self-consistent field theory have been promoted as a theoretical alternative to study the polymer dynamics on the relevant mesoscopic length and time scales.

In a DDFT, the dynamics of an inhomogeneous polymer system is described by a diffusive equation in the monomer densities

$$\frac{\partial \rho_\alpha(\mathbf{r},t)}{\partial t} = \sum_\beta \nabla_r \left[\int d\mathbf{r}' \Lambda_{\alpha\beta}(\mathbf{r},\mathbf{r}') \nabla_{r'} \mu_\beta(\mathbf{r}',t) \right] \quad (1)$$

Here, $\rho_\alpha(\mathbf{r},t)$ is the density of monomers of type α, $\Lambda_{\alpha\beta}(\mathbf{r},\mathbf{r}')$ is the mobility matrix and $-\nabla_{r'}\mu_\beta(\mathbf{r}',t)$ a local thermodynamic force acting on monomers of type β. The matrix $\underline{\underline{\Lambda}}(\mathbf{r},\mathbf{r}')$ relates the monomer density current to the thermodynamic driving force[44] and depends on the monomer−monomer correlations in the system. The field $\mu_\beta(\mathbf{r},t)$ can be interpreted as a local chemical potential for unconnected monomers of type β and is derived from a free energy functional F, (i.e., $\mu_\beta(\mathbf{r}',t) = \delta F/\delta\rho_\beta(\mathbf{r}',t)$), which is typically taken from self-consistent field (SCF) theory. Since $\rho_\alpha(\mathbf{r},t)$ are coarse-grained quantities, their dynamic evolution equations describe the kinetics in the system on mesoscopic scales. A typical SCF

Received: January 20, 2020
Revised: March 31, 2020
Published: April 20, 2020

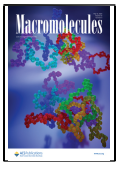

https://dx.doi.org/10.1021/acs.macromol.0c00130
Macromolecules 2020, 53, 3409−3423

theory[45−47] for polymers retains microscopic information on the chain architectures. This combination of mesoscopic and microscopic aspects makes DDFT a promising technique in the pursuit of studying polymer dynamics in an inhomogeneous system. DDFT has been used to explore the kinetic pathways for micelle to vesicle transition in the micellar solutions,[48,49] morphological transitions in the diblock copolymer melts[50−52] and also scaling laws for the polymer interdiffusion during interfacial broadening in the polymer blends.[53−56] DDFT models have also been extended to study the effects of hydrodynamics[57,58] and reptation.[59,60] Recent investigations have also used DDFT in conjunction with the string method[61] to determine the mean free-energy path for pore formation and rupture in cell membranes.[62]

Although DDFT has significantly advanced our understanding of polymer dynamics, it suffers from the problem that DDFT models are typically constructed in an ad hoc manner. The dynamics of polymers is well-known to be governed by relaxation processes on multiple time scales.[63] When projecting the dynamical equations for monomer coordinates onto a dynamical equation for densities such as eq 1 in a systematic manner, for example, using the Mori-Zwanzig formalism,[64,65] this invariably results in a generalized Langevin equation with a memory kernel.[66] In DDFT, the memory kernel is replaced by one single, time independent (but nonlocal) effective mobility function. This greatly increases the computational efficacy of the resulting coarse-grained model, however, the optimal way to choose such an effective mobility is not clear.

Currently, all approaches in the literature are based on heuristic assumptions. For chains in the Rouse regime, these approximate schemes can broadly be categorized into local and nonlocal approaches.[67] In the local approach, monomers are assumed to diffuse in the system independent of each other. In the nonlocal approaches, polymers are assumed to diffuse as a whole. These approximations significantly reduce the complexity in handling the DDFT equation. However, they come with their own caveats. Most importantly, it was found that the choice of DDFT approach may influence the pathways of self-assembly that are observed in DDFT calculations. One example is the dynamics of vesicle formation from homogeneous nucleation, where nonlocal DDFT calculations predicted the existence of competing pathways of self-assembly[48,49] (which was then confirmed both by experiments[68−70] and simulations[71−74]), whereas only one pathway was present in local DDFT simulations.[75] Moreover, local DDFT calculations greatly overestimate the frequency of vesicle fusion events,[76] which are largely suppressed in nonlocal DDFT simulations[77,78] consistent with experiments.[69] When comparing to particle-based simulations, local DDFT calculations generally tend to overestimate the speed of structure formation, and nonlocal DDFT calculations tend to underestimate it.[56,67,76]

It should be noted that none of these approaches incorporate knowledge on the microscopic dynamics in the underlying polymer dynamics. In recent years, bottom-up coarse-graining techniques have become increasingly popular in materials science, where coarse-grained models are constructed from fine-grained simulations in a systematic manner. Examples are techniques for deriving effective potentials in coarse-grained models[79−83] or effective friction coefficients[84] or even memory kernels[85−92] in dynamical equations. Since SCF models bridge between microscopic and the mesoscopic length scales, it should be possible to apply similar ideas for the construction of DDFT equations in order to improve their predictive capabilities.

In this article, we explore two physically motivated bottom-up construction schemes for determining DDFT mobility functions $\Lambda(\mathbf{r}, \mathbf{r}')$ from microscopic simulations. In the first approach, we follow a classical approach to this type of problem and consider the Green−Kubo relation[93−95] that relates $\Lambda(\mathbf{r}, \mathbf{r}')$ to an integral over an appropriate current−current time correlation function. Unfortunately, the result turns out to be not very useful, for reasons that we shall discuss below. In a second approach, we therefore propose to extract $\Lambda(\mathbf{r}, \mathbf{r}')$ from the characteristic relaxation time of the dynamic structure factor of single chains.

To test our approach, we study two related problems. The first is the dynamics associated with the formation of the lamellar structure in diblock copolymer melts, and the second is the relaxation of a lamellar structure into a homogeneous state. We specifically choose these problems because existing local and nonlocal DDFT schemes are known to significantly under- or overestimate the time scales of (dis)ordering in comparison to fine-grained simulations of the same systems. We show that the bottom-up constructed DDFT models are able to capture both the global dynamics and the relaxation due to local rearrangements of the chain at the relevant length scales. This significantly improves the DDFT predictions for the above listed problems.

The rest of the manuscript is organized as follows: In the next section, we first introduce the general framework of DDFT theory and briefly describe the Ansätze for mobility functions that have been proposed in the literature. Then we present and discuss our two bottom-up approaches. Finally, in the fourth section, we apply the approach to the study of ordering and disordering in diblock copolymer melts. We conclude with a summary and an outlook.

2. GENERAL FRAMEWORK OF DDFT

The dynamic density functional theory is an extension of the classical density functional theory, where the equilibrium free energy of a many-body system is expressed as a functional of coarse-grained field variables, the density fields.[94,96,97] A mathematical basis for this formalism is provided by the Hohenberg−Kohn theorem.[98,99] Here we consider polymer systems with different types of monomers α, hence our free energy functional depends on several fields, $F(\{\rho_\alpha\})$. In practice, we will use the functional provided by the self-consistent field (SCF) theory,[45−47] which is a mean-field approach.

The objective of the DDFT is to construct a physically motivated scheme for the dynamical evolution of the microscopic densities, based on the given static functional. Such a scheme is expected to drive the system along a path of low free energy with meaningful dynamic information, in order to reach the equilibrium state or at least a metastable minimum of F. Since the density is a conserved field, its longest-wavelength Fourier components are slowly relaxing variables.[47] This motivates the construction of a diffusive equation that involves the dynamic evolution of density fields only, resulting in so-called model B dynamics according to the classification of Hohenberg and Halperin.[100]

A simple popular Ansatz is to assume the linear instantaneous form

https://dx.doi.org/10.1021/acs.macromol.0c00130
Macromolecules 2020, 53, 3409−3423

$$\frac{\partial \rho_\alpha(\mathbf{r}, t)}{\partial t} = \nabla_r \sum_\beta \int d\mathbf{r}' \Lambda_{\alpha\beta}(\mathbf{r}, \mathbf{r}') \nabla_{\mathbf{r}'} \mu_\beta(\mathbf{r}', t) \tag{2}$$

with $\mu_\beta(\mathbf{r}, t) = \delta F/\delta \rho_\beta(\mathbf{r}, t)$. The mobility function $\Lambda_{\alpha\beta}(\mathbf{r}, \mathbf{r}')$ relates the density current of the monomer α at position $\mathbf{r}$ to the thermodynamic driving force $(-\nabla \mu_\beta)$ on the monomer β at position $\mathbf{r}'$. In the present paper, we will consider single-component homopolymer or copolymer melts with average monomer density ρ_0 and assume that all chains have equal length N. Furthermore, to simplify the notation we will often use reduced quantities $\phi_\alpha = \rho_\alpha/\rho_0$, $\hat{\mu}_\beta = \frac{N}{\rho_0}\delta F/\delta \phi_\beta = N\mu_\beta$, and $\hat{\Lambda} = \Lambda/\rho_0 N$, which allows us to rewrite eq 2 as

$$\frac{\partial \phi_\alpha(\mathbf{r}, t)}{\partial t} = \nabla_r \sum_\beta \int d\mathbf{r}' \hat{\Lambda}_{\alpha\beta}(\mathbf{r}, \mathbf{r}') \nabla_{\mathbf{r}'} \hat{\mu}_\beta(\mathbf{r}', t) \tag{3}$$

We note that the instantaneous assumption is questionable in polymeric systems, which are known to exhibit memory effects,[63] as already discussed in the introduction. In DDFT, one implicitly assumes that the memory kernel can be replaced by a simple, time-independent (but not necessarily local) function. A second important approximation, which is typically made in polymeric DDFT approaches and which we will also adopt here, is a mean-field approximation. In the spirit of the SCF theory, which provides the static density functional F, polymers are assumed to move independently in an external field provided by the other polymers. This field may include hydrodynamic flows and even entanglements, but only in an averaged sense. Hence the mobility function Λ describes the mobility of individual chains. It includes effects of intrachain monomer correlations but not those of interchain correlations. From eq 2, one can thus extract a mobility function per chain, given by $\Lambda^{(s)} = \Lambda N/\rho_0 = \hat{\Lambda} N^2$.

For melts in the Rouse regime (i.e., chains are non-entangled), three types of Ansatz for the mobility coefficients have been proposed in the literature:

i. Local Coupling Scheme. In this approximation, monomer beads are assumed to diffuse independently of each other with the mobility D_0/k_BT.[38] This leads to the following expression for $\hat{\Lambda}_{\alpha\beta}(\mathbf{r}, \mathbf{r}')$

$$\hat{\Lambda}_{\alpha\beta}^{\text{Local}}(\mathbf{r}, \mathbf{r}') = \frac{D_0}{N k_B T} \phi_\alpha(\mathbf{r}) \delta_{\alpha\beta} \delta(\mathbf{r} - \mathbf{r}') \tag{4}$$

ii. Chain Coupling Schemes. These approaches assume that the internal structure of the polymer chain relaxes on a time scale much faster than the collective motion of the chain. As a consequence, the polymer chains are assumed to diffuse as a whole with the mobility $D_c = D_0/N$. For this case, Maurits et al. have derived the expression[59]

$$\hat{\Lambda}_{\alpha\beta}^{\text{Chain}}(\mathbf{r}, \mathbf{r}', t) = \frac{D_c}{k_B T} \frac{P_{\alpha\beta}(\mathbf{r}, \mathbf{r}', t)}{\rho_0 N} \tag{5}$$

where $P_{\alpha\beta}(\mathbf{r}, \mathbf{r}', t)/\rho_0 N$ is the pair correlation of monomers α, β on the same chain at position $\mathbf{r}$ and $\mathbf{r}'$, normalized to the integral one. Within the SCF theory, this quantity can be calculated exactly using a scheme proposed earlier by two of us.[67] Further approximations have been proposed, such as the external potential dynamics (EPD) approximation (not discussed here) and the Debye approximation, which approximates $P_{\alpha\beta}/\rho_0$ by the pair correlations of ideal Gaussian chains, that is, the Debye correlation function[63]

$$\hat{\Lambda}_{\alpha\beta}^{\text{Debye}}(\mathbf{r}, \mathbf{r}') = \frac{D_c}{N k_B T} g_{\alpha\beta}(\mathbf{r} - \mathbf{r}') \tag{6}$$

Analytical expressions are available for the Fourier representation of $g(\mathbf{r} - \mathbf{r}')$. For example, for diblock copolymers one obtains[47,101]

$$g_{\alpha\alpha}(q) = N f_D(h_\alpha, x)$$
$$g_{AB} = \frac{N}{2}\{f_D(1, x) - f_D(h_A, x) - f_D(h_B, x)\} \tag{7}$$

where $x = q^2 R_g^2$, h_α is the fraction of block α, and $f_D(h, x) := \frac{2}{x^2}(hx + e^{-hx} - 1)$ is the Debye function.

iii. Mixed Coupling Scheme. The predictions of DDFTs based on local or nonlocal schemes have been compared to simulations, and both were found to have shortcomings.[56,67] In a previous paper,[67] two of us have therefore proposed a mixed scheme where the dynamics is assumed to be governed by a local mobility function on short wavelengths and a nonlocal one on large wavelengths. To this end, a filter function $\Gamma(\mathbf{r})$ was introduced that filters out the long-wavelength part of the thermodynamic driving force via a convolution integral

$$\hat{f}_\alpha^{\text{Nonlocal}}(\mathbf{r}) = -\int d\mathbf{r}' \Gamma(|\mathbf{r} - \mathbf{r}'|) \nabla \hat{\mu}_\alpha(\mathbf{r}') \tag{8}$$

with

$$\Gamma(r) = (2\pi\sigma^2)^{-3/2} \exp\left\{\frac{-r^2}{2\sigma^2}\right\} \tag{9}$$

This "coarsened" force is then taken to drive nonlocal chain diffusion, whereas the remaining part

$$\hat{f}_\alpha^{\text{Local}}(\mathbf{r}) = -\nabla \hat{\mu}_\alpha(\mathbf{r}) - \hat{f}_\alpha^{\text{Nonlocal}}(\mathbf{r}) \tag{10}$$

drives local rearrangements of the chain via a local mobility coefficient. The resulting interpolated scheme has the form

$$\frac{\partial \phi_\alpha}{\partial t} = -\nabla \sum_\beta \int d\mathbf{r}' [\hat{\Lambda}_{\alpha\beta}^{\text{Nonlocal}}(\mathbf{r}, \mathbf{r}') \hat{f}_\beta^{\text{Nonlocal}}(\mathbf{r}') + \hat{\Lambda}_{\alpha\beta}^{\text{Local}}(\mathbf{r}, \mathbf{r}') \hat{f}_\beta^{\text{Local}}(\mathbf{r}')] \tag{11}$$

where $\hat{\Lambda}^{\text{Nonlocal}}$ can be any of the chain coupling schemes discussed above. The tunable parameter σ determines the length scale of crossover between the local and the nonlocal dynamics. When referring to mixed scheme DDFT calculations in the present paper, these are carried out by mixing local and Debye dynamics with the filter parameter $\sigma = 0.3R_g$, a value found to be optimal in our previous work.[67]

3. APPROACHES TO DETERMINE DDFT MOBILITY COEFFICIENTS FROM MICROSCOPIC SIMULATIONS

The expressions for the mobility coefficients discussed in the previous section were postulated more or less heuristically without much input on the underlying microscopic dynamics. The only parameters that can be used to match the microscopic and the DDFT dynamics are the diffusion constant and, in case of the mixed scheme, the tuning parameter σ. The purpose of the present work is to derive more informed bottom-up schemes, where the mobility coefficients are calculated from simulations of a microscopic reference system. We have explored two such approaches which we will now discuss below.

https://dx.doi.org/10.1021/acs.macromol.0c00130
Macromolecules 2020, 53, 3409−3423

In both cases, we will assume that our system is homogeneous, hence $\Lambda(\mathbf{r}, \mathbf{r}')$ is translationally invariant. We can then conveniently rewrite the DDFT equations in Fourier representation as

$$\partial_t \rho_\alpha(\mathbf{q}, t) = -q^2 \sum_\beta \Lambda_{\alpha\beta}(\mathbf{q}) \mu_\beta(\mathbf{q}, t) \tag{12}$$

with $\mu_\beta(\mathbf{q}, t)/V = \delta F/\delta \rho_\beta(-\mathbf{q}, t)$. Here and throughout, we define the Fourier transform via[63]

$$f(\mathbf{q}) = \int d\mathbf{r} e^{i\mathbf{q}\cdot\mathbf{r}} f(\mathbf{r}), \quad f(\mathbf{r}) = \frac{1}{V}\sum_{\mathbf{q}} \mathrm{e}^{-i\mathbf{q}\cdot\mathbf{r}} f(\mathbf{q})$$

3.1. Green−Kubo Approach. The first approach is based on the Green−Kubo formalism, which is a standard tool to determine transport coefficients from simulations. Let us first recapitulate the general formalism.[94,95,102] For a given microscopic system with Hamiltonian H, we consider the linear response of a quantity $\dot{A}$ to a perturbation of H caused by a generalized field Z_B that couples to a quantity B (i.e., $H = H_0 - Z_B B$). According to the Green−Kubo formalism, the response is given by $\langle \dot{A} \rangle = \lambda_{AB} Z_B$ with $\lambda_{AB} = -\frac{1}{k_B T}\int_0^\infty \mathrm{d}t \langle \dot{A}(t)\dot{B}(0)\rangle$ in classical systems.

To apply this formalism to our DDFT problem, we choose $A = \rho_\alpha(\mathbf{q}, t)$ and $B = \rho_\beta(\mathbf{q}, t)$, where $\rho_\zeta(\mathbf{q}, t)$ (with $\zeta = \alpha, \beta$) is derived from the monomer coordinates $\mathbf{R}_k(t)$ via $\rho_\zeta(\mathbf{q}, t) = \sum_k e^{i\mathbf{q}\cdot\mathbf{R}_k(t)} \gamma_k^{(\zeta)}$ with $\gamma_k^{(\zeta)} = 1$ if monomer k is of type ζ, and $\gamma_k^{(\zeta)} = 0$ otherwise. This results in $\dot{A} = i\mathbf{q}\cdot\mathbf{j}_\alpha(\mathbf{q}, t)$ and $\dot{B} = -i\mathbf{q}\cdot\mathbf{j}_\beta(\mathbf{q}, t)$ with $\mathbf{j}_\zeta(\mathbf{q}, t) = \sum_k e^{i\mathbf{q}\cdot\mathbf{R}_k(t)} \dot{\mathbf{R}}_k(t) \gamma_k^{(\zeta)}$. The continuity equation for ρ_α in Fourier representation reads $\partial_t \rho_\alpha(\mathbf{q}, t) = i\mathbf{q}\cdot\mathbf{j}_\alpha(\mathbf{q}, t) = \dot{A}$. From eq 12, we hence know $\dot{A} = -q^2 \sum_\beta \Lambda_{\alpha\beta}(\mathbf{q}) \mu_\beta(\mathbf{q})$, where $(-\mu_\beta(\mathbf{q}, t)/V)$ couples to B. Now, in the linear response regime an external field Z_B coupling to B would contribute additively to $(-\mu_\beta(\mathbf{q}, t)/V)$ and generate the same response, hence we can identify $\Lambda_{\alpha\beta} = \lambda_{AB}/q^2 V$ and the Green−Kubo formalism results in the following expression

$$\Lambda_{\alpha\beta}(\mathbf{q}) = \frac{1}{V k_B T}\int_0^\infty \mathrm{d}t \langle \mathbf{j}_\alpha(\mathbf{q}, t)\mathbf{j}_\beta(-\mathbf{q}, 0)\rangle : \hat{\mathbf{q}}\hat{\mathbf{q}} \tag{13}$$

with $\hat{\mathbf{q}} = \mathbf{q}/q$ and the tensor products $\mathbf{jj}$ and $\hat{\mathbf{q}}\hat{\mathbf{q}}$.

However, the numerical evaluation of this expression and a theoretical analysis for the special case of Rouse chains shows that eq 13 yields zero for all nonzero $\mathbf{q}$. This is demonstrated in more detail in the appendix. Only at $\mathbf{q} = 0$ do we recover the familiar Green−Kubo expression for the diffusion constant.

The reason becomes clear if we recall the premises underlying the Green−Kubo relations. They describe the response of stationary currents to generalized thermodynamic forces. In our case, at $q \neq 0$ a stationary current is not possible, since it would generate indefinitely growing density fluctuations $\rho(\mathbf{q}, t)$. Since $\rho(\mathbf{q}, t)$ must saturate eventually, the flows $\mathbf{j}(\mathbf{q}, t)$ will average to zero at late times, independent of the applied generalized forces. Therefore, the Green−Kubo transport coefficients must vanish for any nonzero $\mathbf{q}$. Stationary currents are only possible at $\mathbf{q} = 0$. Hence the Green−Kubo formalism is not suitable for determining $\mathbf{q}$-dependent mobility functions for DDFT models.

In fact, this problem is not uncommon in applications of Green−Kubo integrals.[103,104] For example, confinement can prevent stationary currents, which is why Green−Kubo integrals may vanish in confined systems, even if locally a description in terms of a Markovian dynamical equations with well-defined transport coefficients is appropriate. The $\mathbf{q}$-dependent Green−Kubo integrals considered here, which describe the response to a spatially varying field, vanish for a similar reason. One popular solution to this problem has been to assume that the time scales of local Markovian dynamics and global constrained dynamics are well separated and to search for a plateau in the running Green−Kubo integrals. In our case, however, the running integrals do not exhibit a well-defined plateau (data not shown). We will discuss this point further in Section 5.

3.2. Relaxation Time Approach. In the present subsection, we describe an alternative approach to deriving DDFT mobility coefficients from microscopic trajectories: We propose to estimate them directly from the characteristic relaxation time of the single chain dynamic structure factor.

To motivate our Ansatz, we begin with discussing some implications of the DDFT equations. We consider the dynamics of a single tagged chain s with corresponding monomer density $\rho_\alpha^{(s)}$. In the mean-field spirit, the DDFT equation for $\rho_\alpha^{(s)}$ in Fourier representation takes the form

$$\partial_t \rho_\alpha^{(s)}(\mathbf{q}, t) = -q^2 \sum_\beta \Lambda_{\alpha\beta}^{(s)}(\mathbf{q}) \mu_\beta^{(s)}(\mathbf{q}, t) \tag{14}$$

where $\Lambda^{(s)} = \hat{\Lambda} N^2$ is the mobility per chain, and $\mu_\beta^{(s)}(\mathbf{q}) = V\delta F^{(s)}/\delta \rho_\beta^{(s)}(-\mathbf{q})$ is derived from the free energy $F^{(s)}$ of a single chain that moves independently in the averaged background provided by the other chains. Next we multiply both sides with $\rho_\gamma^{(s)}(-\mathbf{q}, 0)$ and average over chain conformations. Identifying $g_{\alpha\gamma}(\mathbf{q}, t) = \frac{1}{N}\langle \rho_\alpha^{(s)}(\mathbf{q}, t)\rho_\gamma^{(s)}(-\mathbf{q}, 0)\rangle$, we obtain

$$\partial_t g_{\alpha,\gamma}(\mathbf{q}, t) = -\frac{q^2}{N}\sum_\beta \Lambda_{\alpha\beta}^{(s)}(\mathbf{q}) \langle \mu_\beta^{(s)}(\mathbf{q}, t)\rho_\gamma^{(s)}(-\mathbf{q}, 0)\rangle \tag{15}$$

To proceed, we expand $F^{(s)}$ in powers of $\rho^{(s)}(\mathbf{q})$, giving

$$F^{(s)} = \text{const.} + \frac{k_B T}{2NV}\sum_{\mathbf{q}} \underline{\rho}^{(s)}(-\mathbf{q}) \underline{\underline{g}}^{-1}(\mathbf{q}, 0) \underline{\rho}^{(s)}(\mathbf{q}) + \cdots \tag{16}$$

Here and in the following, we use a matrix notation for convenience, that is, $\underline{\rho} \triangleq (\rho_\alpha)$, $\underline{\underline{\Lambda}} \triangleq (\Lambda_{\alpha\beta})$, and so forth. Taking the derivative with respect to $\rho_\beta^{(s)}(-\mathbf{q})$, we obtain $\underline{\mu}^{(s)}(\mathbf{q}) \approx k_B T \frac{1}{N}\underline{\underline{g}}^{-1}(\mathbf{q})\underline{\rho}^{(s)}(\mathbf{q})$. Inserting this in eq 15 yields

$$\partial_t \underline{\underline{g}}(\mathbf{q}, t) \approx -\frac{k_B T q^2}{N}\underline{\underline{\Lambda}}^{(s)}(\mathbf{q}) \underline{\underline{g}}^{-1}(\mathbf{q}, 0) \underline{\underline{g}}(\mathbf{q}, t) \tag{17}$$

which can be solved in matrix form, giving

$$\underline{\underline{g}}(\mathbf{q}, t) = \exp\left(-\frac{k_B T q^2}{N}\underline{\underline{\Lambda}}^{(s)}(\mathbf{q}) \underline{\underline{g}}^{-1}(\mathbf{q}, 0) t\right) \underline{\underline{g}}(\mathbf{q}, 0) \tag{18}$$

This equation approximates the relaxation of the single chain under three assumptions: (i) memory effects were neglected (the basis of the DDFT approach), (ii) a mean-field approximation was made (in eq 14), and (iii) density fluctuations were assumed to be small (in eq 16). Within these approximations, the relaxation of the chain is determined by a $\mathbf{q}$-dependent "relaxation time matrix" $\underline{\underline{T}}(\mathbf{q})$, $\underline{\underline{g}}(\mathbf{q}, t) = \exp(-t\underline{\underline{T}}^{-1}(\mathbf{q}))\underline{\underline{g}}(\mathbf{q}, 0)$ and, using $\underline{\underline{\Lambda}}^{(s)} = \hat{\underline{\underline{\Lambda}}} N^2$, we can identify

https://dx.doi.org/10.1021/acs.macromol.0c00130
Macromolecules 2020, 53, 3409−3423

$$\hat{\underline{\underline{\Lambda}}}(\mathbf{q}) = \frac{1}{k_B T q^2 N} \underline{\underline{T}}^{-1}(\mathbf{q}) \underline{\underline{g}}(\mathbf{q}, 0) \tag{19}$$

We can further simplify this expression by assuming that the relaxation of the chain is governed by a single $\mathbf{q}$-dependent time constant $\tau(\mathbf{q})$, that is, $\underline{\underline{T}}(\mathbf{q}) \approx 1 \cdot \tau(\mathbf{q})$. Then eq 19 can be rewritten as

$$\hat{\underline{\underline{\Lambda}}}(\mathbf{q}) = \frac{1}{k_B T q^2 N \tau(\mathbf{q})} \underline{\underline{g}}(\mathbf{q}, 0) \tag{20}$$

The considerations above suggest the following procedure to determine an effective mobility coefficient for the DDFT model: We first conduct fine-grained simulations of the polymer melt in a homogeneous reference system (i.e., in the case of the diblock copolymer melt, below the order−disorder transition (ODT)). From the simulation trajectory for the full $g(\mathbf{q}, t)$, we compute the relaxation time $\tau(\mathbf{q})$ and insert it in eq 19 or eq 20.

The question remains how to define the characteristic relaxation time. This question is nontrivial, because the actual behavior of $g(\mathbf{q}, t)$ is driven by a multitude of time scales, corresponding to the different internal modes of the chain. At late times, the slowest diffusive mode dominates, and $g(\mathbf{q}, t)$ has the limiting behavior[63] $\lim_{t\to\infty} g(\mathbf{q}, t) \propto \exp(-D_c q^2 t)$, giving $\tau = 1/D_c q^2$. Inserting this in eq 20, we recover the Ansatz of nonlocal Debye dynamics, (see eq 6) $\hat{\underline{\underline{\Lambda}}}(\mathbf{q}) = \frac{D_c}{N k_B T} \underline{\underline{g}}(\mathbf{q})$.

However, by the time when this limiting behavior sets in, much of the structuring has already taken place. It would be more desirable to define $\tau(\mathbf{q})$ such that it captures the dominant time scales of structure formation on the scale $\mathbf{q}$. In the present work, we test two prescriptions for determining τ and then calculate $\hat{\underline{\underline{\Lambda}}}$ via eq 20

$$\hat{\underline{\underline{\Lambda}}}^{\tau_R}: \quad \text{from} \quad \tau_R = \frac{1}{g(\mathbf{q}, 0)} \int_0^\infty \mathrm{d}t\, g(\mathbf{q}, t) \tag{21}$$

$$\hat{\underline{\underline{\Lambda}}}^{\tau_e}: \quad \text{from} \quad g(\mathbf{q}, t = \tau_e) \stackrel{!}{=} g(\mathbf{q}, 0)/e \tag{22}$$

where e is the Euler number and $g(\mathbf{q}, t)$ is the full single-chain structure factor

$$g(\mathbf{q}, t) = \sum_{\alpha,\beta} g_{\alpha\beta}(\mathbf{q}, t) \tag{23}$$

In a third approach, we generalize eq 21 to extract a full relaxation time matrix

$$\hat{\underline{\underline{\Lambda}}}^{T}: \quad \text{from} \quad \underline{\underline{T}}(\mathbf{q}) = \int_0^\infty \mathrm{d}t\, \underline{\underline{g}}(\mathbf{q}, t) \underline{\underline{g}}^{-1}(\mathbf{q}, 0) \tag{24}$$

and use that to determine $\hat{\underline{\underline{\Lambda}}}$ via eq 19. Calculating $\hat{\underline{\underline{\Lambda}}}$ with this method involves matrix inversions and multiplications for every value of $\mathbf{q}$. However, in the case of symmetric A/B diblock copolymers with fully equivalent A and B blocks, the prescription can be simplified. For symmetry reasons, $\underline{\underline{g}}$, $\underline{\underline{T}}$ and $\hat{\underline{\underline{\Lambda}}}$ then have the same matrix structure ($M_{\alpha\beta}$) with $M_{AA} = M_{BB}$, $M_{AB} = M_{BA}$ and thus share the same Eigenvectors, (1, 1) and (1, −1). Using these to diagonalize $\underline{\underline{g}}$ and $\underline{\underline{T}}$, we obtain

$$\hat{\Lambda}_{AA}(\mathbf{q}) = \frac{1}{4 k_B T q^2 N} \left(\frac{g(\mathbf{q}, 0)}{\tau_R} + \frac{\Delta(\mathbf{q}, 0)}{\tau_\Delta} \right) \tag{25}$$

$$\hat{\Lambda}_{AB}(\mathbf{q}) = \frac{1}{4 k_B T q^2 N} \left(\frac{g(\mathbf{q}, 0)}{\tau_R} - \frac{\Delta(\mathbf{q}, 0)}{\tau_\Delta} \right) \tag{26}$$

with $g(\mathbf{q}, t)$ and τ_R defined as above (eqs 23, 21), $\Delta(\mathbf{q}, t) = g_{AA}(\mathbf{q}, t) + g_{BB}(\mathbf{q}, t) - g_{AB}(\mathbf{q}, t) - g_{BA}(\mathbf{q}, t)$, and $\tau_\Delta = \frac{1}{\Delta(\mathbf{q}, 0)} \int_0^\infty \mathrm{d}t\, \Delta(\mathbf{q}, t)$.

In practice, determining the integrals (eq 21) and (eq 24) by numerical integration of simulation data only is not possible for small q, because the relaxation time diverges for $q \to 0$. Therefore, an extrapolation procedure must be devised. At late times, $g_{\alpha\beta}(\mathbf{q}, t)$ is known to decay exponentially[63] according to $g(\mathbf{q}, t) \sim \exp(-q^2 D_c t)$. Hence we make the Ansatz

$$g_{\alpha\beta}(q, t) = g_{\alpha\beta}(q, t_i)) \exp(-q^2 D_{\text{eff}}(t - t_i)) \tag{27}$$

for large t, t_i with $t > t_i$. Specifically, we fit the data for $g_{\alpha\beta}(q, t)$ to eq 27 in time windows $t \in [t_i, t_f]$, using the weighted least-squares fit module in the Matlab suite[105] and then choose those values of t_{i_f} which yield the value of D_{eff} that is closest to the theoretical value, $D_c = D_0/N$. The integrals over t in eq 21 and eq 24 are then evaluated by first numerically integrating the data up to $t = t_i$, and then using the extrapolation (eq 27) in the integral from $t = t_i$ to infinity. Typical values for t_i, t_f are $t_i \approx 20 t_0$ and $t_f \approx 40 t_0$.

Figure 1 shows results for the q-dependent mobility functions of homopolymers in a homopolymer melt. They

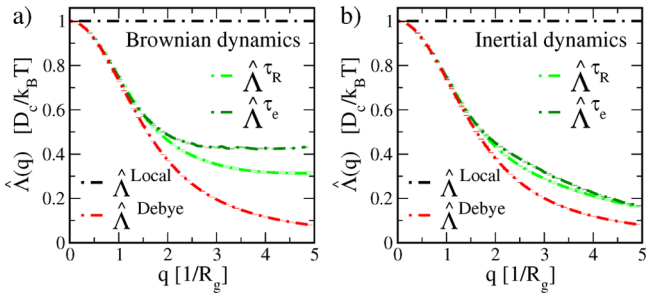

Figure 1. Normalized mobility functions of homopolymers with length $N = 40$ in a melt, as obtained via the relaxation time method (eq 20) with Brownian dynamics (a) and inertial dynamics (b) simulation data. Two prescriptions for determining the single chain relaxation time are tested, τ_R (green, eq 21) and τ_e (blue, eq 22). Also shown for comparison are the results from the Debye and the local approximation ($(\Lambda^{\text{Debye}}(q)$, red) and ($(\Lambda^{\text{Local}}(q)$, black)).

were extracted from Brownian dynamics simulations (massless monomers, Figure 1a) and molecular dynamics simulations (massive monomers, Figure 1b) of melts of Gaussian chains with length $N = 40$, using the prescriptions eq 21 and eq 22. We note that in the case of homopolymers, the prescription eq 24 is equivalent to eq 21. For comparison, we also show the mobility functions corresponding to the local and the Debye approximation. In the local scheme, the mobility is constant; in the Debye scheme, it is proportional to the static structure factor. The results from the relaxation schemes are intermediate between the local and the Debye scheme. At small q, they follow the Debye scheme. At larger q, the mobility is enhanced, hence small wavelength modes relax faster. The effect is more pronounced for Brownian dynamics than for inertial dynamics, most likely because the inertial time scale contributes to the total relaxation time at small wavelengths (see also Figure 10b).

https://dx.doi.org/10.1021/acs.macromol.0c00130
Macromolecules 2020, 53, 3409−3423

Thus, we find that the mobility functions obtained with the relaxation time approach interpolate between the nonlocal mobility function (at small q) and the local mobility function (at larger q). This seems promising, since our previous studies have suggested that such an interpolation may be necessary to capture the kinetics of structure formation in copolymer systems.[67] We will now test our DDFT approach by performing a systematic comparison of fine-grained simulations and DDFT predictions for the ordering/disordering kinetics in block copolymer melts.

4. APPLICATION TO DIBLOCK COPOLYMER MELTS

We consider melts of n_c block copolymers containing N_A beads of type A and N_B beads of type B, in a box of volume $V = L_x \times L_y \times L_z$ with dimension L_i in i direction and periodic boundary conditions. The average monomer density is thus $\rho_0 = n_c N/V$. Polymers are modeled as Gaussian chains, that is, chains of "monomer beads" connected by harmonic springs. The nonbonded monomer interactions are characterized in terms of a Flory–Huggins parameter χ, which controls the incompatibility between A and B monomers, and a Helfand parameter κ, which controls the compressibility.

We carry out fine-grained simulations of order/disorder processes in such systems and compare them with DDFT calculations, using the SCF free energy functional and mobility functions that are extracted from fine-grained simulations at $\chi = 0$.

Throughout this paper, lengths will be represented in units of the radius of gyration R_g of an ideal chain of length $N = N_A + N_B$, energies in units of the thermal energy, k_BT, and time in units of $t_0 = R_g^2/D_0$, where D_0 is the monomer diffusivity.

4.1. Model and Methods. *4.1.1. Fine-Grained Model and Simulation Method.* Since we focus on a comparison of dynamical properties of particle-based and field-based models here, we use as fine-grained model a particle-based implementation of an Edwards model,[106−109] where the nonbonded monomer interactions are described by the same Hamiltonian than that underlying the SCF free energy functional. At sufficiently high polymer density and sufficiently far from critical points, the static properties of such models are known to be well represented by SCF functionals without much parameter adjustment.[67]

Nonbonded interactions are thus expressed as a functional of the local monomer densities.[107] Let $\mathbf{R}_{m,j}$ denote the position of the jth monomer on the mth chain. The Hamiltonian H describing the monomer interactions is then expressed as

$$\frac{H}{k_BT} = \frac{N}{4R_g^2}\sum_{m=1}^{n_c}\sum_{j=1}^{N}(\mathbf{R}_{m,j} - \mathbf{R}_{m,j-1})^2 + \rho_0\chi\int d\mathbf{r}\hat{\phi}_A(\mathbf{r})\hat{\phi}_B(\mathbf{r}) + \rho_0\kappa\int d\mathbf{r}(\hat{\phi}_A(\mathbf{r}) + \hat{\phi}_B(\mathbf{r}) - 1)^2 \quad (28)$$

where the first term represents the bonded interactions in the polymer, and the last two terms correspond to nonbonded interactions. The quantities $\hat{\phi}_\alpha(\mathbf{r})$ are the normalized microscopic densities of α-type beads ($\alpha = A$ or B) at position $\mathbf{r}$, defined as, $\hat{\phi}_\alpha(\mathbf{r}) = \frac{1}{\rho_0}\sum_{mj}\delta(\mathbf{r} - \mathbf{R}_{mj})\delta_{\alpha,\tau_{mj}}$, where $\tau_{mj} = A$ or B characterizes the monomer sequence on chain m.

In practice, the local densities are evaluated on a grid with grid size $\Delta x = \Delta y = \Delta z = 0.1R_g$, using a first order cloud in the cell (CIC) scheme.[110] The grid size is an important ingredient of the model definition, as it sets the range of nonbonded interactions. In the simulations, we consider systems with average monomer density $\rho_0 = \frac{2}{3} \times 10^5/R_g^3$, that is, roughly 50 monomers per grid cell. For this choice of densities and grid parameters, grid artifacts[111,112] are negligible, and the renormalized values of χ and κ in the SCF theory are practically identical to the corresponding "bare" parameters in eq 28.[112] Furthermore, fluctuation effects are small. The strength of thermal fluctuations can be characterized by the Ginzburg parameter,[42,47] $C^{-1} = V/n_cR_g^3$. In our system, this parameter is $C^{-1} = 0.01$ or less.

Monomers (m, j) with mass $M_{m,j}$ evolve in time according to a Langevin equation

$$M_{m,j}\dot{\mathbf{v}}_{m,j}(t) = -\frac{\partial H}{\partial \mathbf{R}_{m,j}} - \Gamma\mathbf{v}_{m,j} + \sqrt{2\Gamma k_BT}\,\mathbf{f}_{m,j}(t) \quad (29)$$

The first term on the right-hand side describes the conservative interaction forces, the second term corresponds to a friction force (with $\mathbf{v} = d\mathbf{R}/dt$ and the monomer friction $\Gamma = 1/D_0$), and the last term to a stochastic force representing the effect of thermal fluctuations, where $\mathbf{f}_{mj}(t)$ is a Gaussian distributed random noise with zero mean and variance $\langle \mathbf{f}_{mj}(t)\mathbf{f}_{nk}(t')\rangle = \delta_{mn}\delta_{jk}1\delta(t - t')$. Hydrodynamic interactions are thus neglected, and since the interaction potentials defined by eq 28 are soft, entanglement effects are not included as well. We consider the two cases $M_{m,j} \equiv 1k_BTt_0^2/R_g^2$ (inertial dynamics) and $M_{m,j} \to 0$ (overdamped dynamics). In the second case, eq 29 is replaced by

$$\frac{d\mathbf{R}_{m,j}}{dt} = -D_0\frac{\partial H}{\partial \mathbf{R}_{m,j}} + \sqrt{2D_0k_BT}\,\mathbf{f}_{m,j}(t) \quad (30)$$

The equations of motion are integrated using the Velocity–Verlet scheme[113,114] in the case of inertial dynamics (eq 29), and the Euler–Maruyama[113] algorithm in the case of overdamped dynamics (eq 30) with the time step $\delta t = 0.001t_0$.

Specifically, we consider copolymer melts in a simulation box of size $R_g \times R_g \times 3R_g$. Unless stated otherwise, we consider symmetric copolymers, that is, $N_A = N_B$, with total length $N = 40$. For comparison, we also study copolymers with length $N = 20$ or $N = 100$ and vary the A/B fraction. In all cases the monomer density is kept fixed at $\rho_0 = \frac{2}{3} \times 10^5/R_g^3$. The Helfand parameter is set to $\kappa N = 100$. The systems are initially prepared by growing polymers at randomly picked points in the simulation box. In three independent runs, configurations are then equilibrated for 300 000 time steps each. Data for $g(\mathbf{q}, t)$ are subsequently collected over 200 000 time steps and used to extract the mobility functions. In a set of additional simulations, we monitor the formation of lamellar structure in the melt after a step change from $\chi N = 0$ to a finite χN above the ODT, and the decay of the lamellar structure after a step change from finite χN to $\chi N = 0$. The systems are equilibrated as described above and the time evolution is then monitored over 100 000 time steps in 10 independent runs.

4.1.2. SCF Free Energy Functional. As discussed earlier, we use the SCF theory to construct the free energy functional in our DDFT equations. The SCF theory is one of the most powerful equilibrium theories for inhomogeneous polymer systems and has been well documented elsewhere.[45−47,115] Here, we just briefly summarize the main equations, adjusted to our system. We model the copolymers as continuous

https://dx.doi.org/10.1021/acs.macromol.0c00130
Macromolecules 2020, 53, 3409−3423

Gaussian chains,[46,115] and parametrize the contour length by a continuous variable $s \in [0{:}1]$. The free energy functional $F[\{\phi_\alpha(\mathbf{r})\}]$ of our block copolymer system is expressed as

$$\frac{F}{k_BT} = \frac{\rho_0}{N}\Big\{\int d\mathbf{r}[\chi N\phi_A(\mathbf{r})\phi_B(\mathbf{r}) + \kappa N(\phi_A(\mathbf{r}) + \phi_B(r) - 1)^2] - \sum_{\alpha=A,B}\int d\mathbf{r}\phi_\alpha(r)\omega_\alpha(\mathbf{r}) - V \ln Q\Big\} \quad (31)$$

where ϕ_α is the normalized density field of monomers of type α, ω_α is the corresponding conjugate field, and Q is the single chain partition function in the external field ω_α. The conjugate fields are determined implicitly by the requirement

$$\phi_A(\mathbf{r}) = \frac{N_A V}{NQ}\int_0^{N_A/N} ds\, q_f(\mathbf{r}, s)q_b(\mathbf{r}, 1-s)$$
$$\phi_B(\mathbf{r}) = \frac{N_B V}{NQ}\int_0^{N_B/N} ds\, q_b(\mathbf{r}, s)q_f(\mathbf{r}, 1-s) \quad (32)$$

Here $q_f(\mathbf{r},s)$ and $q_b(\mathbf{r},s)$ are the end-integrated forward and backward chain propagators, respectively, which can be obtained from solving the following differential equation

$$\frac{\partial q(\mathbf{r}, s)}{\partial s} = R_g^2\nabla^2 q(\mathbf{r}, s) - \omega(\mathbf{r})q(\mathbf{r}, s) \quad (33)$$

with initial condition $q_{f,b}(\mathbf{r},0) = 1$ and $\omega(\mathbf{r}) = \omega_A(\mathbf{r})$ or $\omega_B(\mathbf{r})$, depending on s: $q_f(\mathbf{r},s)$ is obtained by setting $\omega(\mathbf{r}) = \omega_A(\mathbf{r})$ for $s < N_A/N$ and $\omega(\mathbf{r}) = \omega_B(\mathbf{r})$ otherwise, and $q_b(\mathbf{r},s)$ by setting $\omega(\mathbf{r}) = \omega_B(\mathbf{r})$ for $s < N_B/N$ and $\omega(\mathbf{r}) = \omega_A(\mathbf{r})$ otherwise. Knowing q_f or q_b, one can calculate the single chain partition function Q via

$$Q = \frac{1}{V}\int d\mathbf{r}\; q_f(\mathbf{r}, 1) = \frac{1}{V}\int d\mathbf{r}\; q_b(\mathbf{r}, 1) \quad (34)$$

At equilibrium, $F[\{\phi_\alpha(\mathbf{r})\}]$ assumes a minimum with respect to $\phi_\alpha(\mathbf{r})$, leading to a second set of conditions for the values of the conjugate fields, ω_α

$$\omega_A^{SCF}(\mathbf{r}) = \chi N\phi_B + 2\kappa N(\phi_A + \phi_B - 1)$$
$$\omega_B^{SCF}(\mathbf{r}) = \chi N\phi_A + 2\kappa N(\phi_A + \phi_B - 1) \quad (35)$$

However, in DDFT calculations, these conditions are not imposed. Instead, the system is dynamically driven toward the equilibrium state via the diffusive dynamical eq 3 with $\hat{\mu}_\alpha(\mathbf{r}) = (\omega_\alpha^{SCF}(\mathbf{r}) - \omega_\alpha(\mathbf{r}))$.

The SCF and DDFT calculations in the present work are effectively one-dimensional, that is, we assume that densities vary only in the z-direction. Space is discretized with grid size $\Delta z = 0.1R_g$ The propagator equation, eq 34. is solved using the pseudo spectral scheme[47] with discretization $\Delta s = 0.01$. As in our earlier work,[67] the time step in the DDFT calculations depends on the DDFT scheme. We use $\Delta t = 10^{-4}t_0N$ for DDFT calculations based on Debye dynamics or any of the other predetermined mobility functions $\hat{\Lambda}(\mathbf{r} - \mathbf{r}')$ discussed in Section 3.2, $\Delta t = 10^{-5}t_0N$ for full chain dynamics, eq 5, and $\Delta t = 10^{-6}t_0N$ for local dynamics (eq 4) or mixed dynamics (eq 11).

4.2. Mobility Functions. On the basis of simulations of the fine-grained model discussed above, mobility functions were extracted from the simulation data using the different variants of the relaxation time approaches discussed in Section 3.2. In the following, we will consider melts of symmetric A/B diblock copolymer melts.

Figure 2 shows the results for the full-chain mobility function, $\hat{\Lambda}(q) = \sum_{\alpha\beta}\hat{\Lambda}_{\alpha\beta}(q)$ for different chain lengths (N = 20, 40, 100) at fixed $\chi = 0$, and for different values of χN (χN = 0, 5, 10) at fixed chain length $N = 40$. These values were chosen such that (χN) is still below the value[116,117] $(\chi N)_{ODT} \approx 10.5$ where the order−disorder transition sets in for symmetric diblock copolymers, hence the melt is disordered and isotropic. The behavior of $\hat{\Lambda}(q)$ at $q \to 0$ reflects the translational diffusion of chains and takes the asymptotic value $\hat{\Lambda} = D_c$. Therefore, the curves are rescaled by the chain diffusion constant D_c, which has been calculated independently from the mean-square displacement of the chain. For example, for N = 40, we obtain $D_c^{BD} = (0.0263 \pm 0.0001)R_g^2/t_0$ in Brownian dynamics simulations, and $D_c^{ID} = (0.0224 \pm 0.0003)R_g^2/t_0$ in inertial dynamics simulations, which is close to the value for free Rouse chains, $D_c = 0.025R_g^2/t_0$. Since the interactions between monomers are very soft in the particle-based model, they do not affect the diffusion constant significantly in the disordered phase.

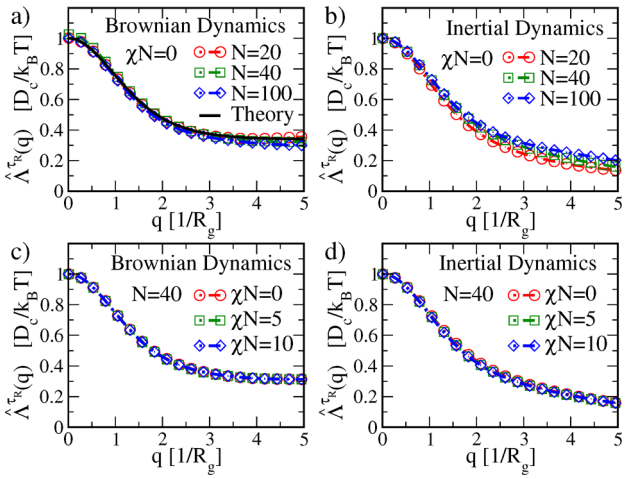

Figure 2. Normalized full-chain mobility function of symmetric A/B copolymers in a melt, as obtained via the relaxation time method (eq 21) from Brownian dynamics simulations (a,c) and inertial dynamics simulation data (b,d) for different chain lengths N or interaction parameter χ as indicated. Solid line in (a) shows theoretical prediction for $N = 40$ obtained by inserting eq 46 into eq 21.

The full-chain mobility function is found to depend weakly on the chain length N (Figure 2a,b), the effects being most pronounced in the regime of high q. If one increases N, the mobility function for high q decreases in the Brownian dynamics case and increases in the inertial dynamics case, such that both mobility functions approach each other. In contrast, the Flory−Huggins parameter χ has practically no influence on the chain mobility function in the disordered regime (Figure 2c,d)). Motivated by this finding, we will use the mobility functions obtained at $\chi = 0$ in all DDFT calculations below.

Next we turn to the discussion of the monomer-species resolved mobility functions $\hat{\Lambda}_{\alpha\beta}$. The results extracted from Brownian dynamics simulation trajectories for symmetric diblock copolymers of length $N = 40$ are shown in Figure 3 for the different relaxation time approaches discussed in Section 3.2. Since $\hat{\Lambda}_{AA}(q) = \hat{\Lambda}_{BB}(q)$ for symmetric systems, and

https://dx.doi.org/10.1021/acs.macromol.0c00130
Macromolecules 2020, 53, 3409−3423

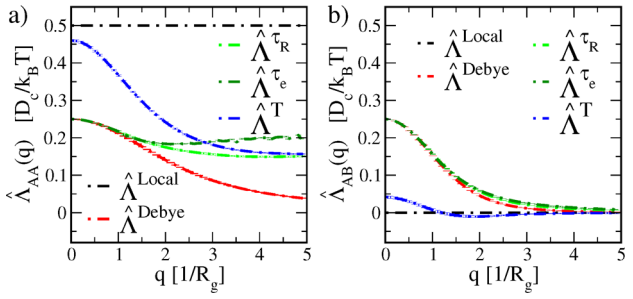

Figure 3. Normalized mobility function $\hat{\Lambda}_{\alpha\beta}$ of symmetric A/B diblock copolymers (length N = 40), obtained from Brownian dynamics simulations at χ = 0, using different variants of the relaxation time method: eqs 21 (light green line), 22 (dark green line), and 24 (blue line). Also shown for comparison is the result from the Debye approximation (red line) and the local approximation in a homogeneous melt (black).

$\hat{\Lambda}_{AB}(q) = \hat{\Lambda}_{BA}(q)$, only the results for $\hat{\Lambda}_{AA}(q)$ and $\hat{\Lambda}_{AB}(q)$ are shown.

If one assumes that the mobility matrix $\underline{\underline{\hat{\Lambda}}}$ is governed by a single relaxation time $\tau(q)$ (eqs 21 or 22), the resulting mobility curves are qualitatively similar to the curves obtained from the Debye approximation (eq 6), except that $\hat{\Lambda}_{\alpha\beta}(q)$ is enhanced at high q values like the full-chain mobility function. However, if one derives $\underline{\underline{\hat{\Lambda}}}$ from a full relaxation time matrix which is calculated according to eq 24, the mobility functions change qualitatively. The intrablock mobility $\hat{\Lambda}^{T}_{AA}(q)$ becomes much larger than in the other nonlocal schemes, especially at small q. Hence monomer rearrangements inside blocks are faster than anticipated in the Debye approximation. Nevertheless, $\hat{\Lambda}^{T}_{AA}(q)$ never reaches the level of the local coupling scheme, where monomers are taken to move independently ($\hat{\Lambda}^{Local}_{AA}(q) = \hat{\Lambda}^{Local}_{BB}(q) \equiv 0.5D_c/k_BT$ for symmetric A/B copolymers in homogeneous melts according to eq 4).

In contrast, the interblock mobility $\hat{\Lambda}^{T}_{AB}(q)$ is much smaller than in the other nonlocal schemes already at q = 0. It then decreases further with increasing q and even becomes slightly negative, until it rises again and reaches zero at large q. We note that the slightly negative values of $\hat{\Lambda}_{AB}(q)$ do not destabilize the system, since the Eigenvalues of $\underline{\underline{\Lambda}}(q)$ are still positive. The interblock mobility is practically zero for q values above $qR_g \approx 1$. The same is obtained with a local approximation, where the motion of A and B monomers is also uncorrelated.

An important consequence is that the values of $\hat{\Lambda}_{AA}(q)$ and $\hat{\Lambda}_{AB}(q)$ at $q \to 0$ differ from each other in the relaxation time matrix scheme $\underline{\underline{\hat{\Lambda}}}^{T}$ (eq 24), whereas they are equal in the other nonlocal schemes. This influences the prediction for the relaxation of composition fluctuations $m(t) = (\Phi_A(t) - \Phi_B(t))/2$. From eq 3, one can derive

$$\partial_t m(\mathbf{q}, t) = -q^2 \frac{1}{2}(\hat{\Lambda}_{AA}(\mathbf{q}) - \hat{\Lambda}_{AB}(\mathbf{q}))\hat{\mu}(\mathbf{q}, t) \tag{36}$$

where $\hat{\mu} = (\hat{\mu}_A - \hat{\mu}_B)$ is conjugate to m. If $m(t)$ is small, one can apply the random phase approximation (RPA)[47,115] and approximate $\hat{\mu}(\mathbf{q},t) \approx \Gamma_2(\mathbf{q})\, m(\mathbf{q},t)$, where the RPA-coefficient $\Gamma_2(\mathbf{q})$ can be identified with the inverse of the collective structure factor of the copolymer melt. Expanding $\Gamma_2(\mathbf{q})$ in powers of q and neglecting compressibility effects, one obtains the leading order[115] $\Gamma_2(\mathbf{q}) \approx 24\, k_BT/q^2R_g^2$ for symmetric diblock copolymers. At small q, eq 37 thus takes the limiting form

$$\partial_t m(\mathbf{q}, t) \approx -\frac{12k_BT}{R_g^2}(\hat{\Lambda}_{AA}(\mathbf{q}) - \hat{\Lambda}_{AB}(\mathbf{q}))m(\mathbf{q}, t) \tag{37}$$

Since $(\hat{\Lambda}_{AA}(0) - \hat{\Lambda}_{AB}(0)) > 0$ in the relaxation time matrix scheme, composition fluctuations are predicted to decay with a finite relaxation time in the limit $q \to 0$. In the other nonlocal schemes, one has $(\hat{\Lambda}_{AA}(0) - \hat{\Lambda}_{AB}(0)) = 0$ at $\mathbf{q} \to 0$, that is, the relaxation time for long-wavelength compositional fluctuations is predicted to diverge. In simulation studies,[66,118] the relaxation time is found to be finite and of order[118] $(2/\pi^2)$ R_g^2/D_c (the Rouse time of the chain), implying $(\hat{\Lambda}_{AA}(0) - \hat{\Lambda}_{AB}(0)) \approx 0.41\, D_c/k_BT$. This is consistent with the data in Figure 3 obtained with the relaxation time matrix method.

4.3. Comparison of DDFT Calculations with Simulations. In order to evaluate the mobility functions discussed in the previous section, we have compared DDFT calculations with fine-grained simulations for different situations of dynamical ordering/disordering in block copolymer melts. In the following, we report the results for Brownian dynamics simulations. The results for inertial dynamics simulations are similar.

4.3.1. Relaxation of an Initially Lamellar Symmetric Diblock Copolymer Melt into the Homogeneous State. In the first example, we study the relaxation of an initially lamellar block copolymer melt into a homogeneous state. Diblock copolymer melts were prepared in a lamellar state by equilibrating them above the order−disorder transition, that is, at $(\chi N)_{init} > (\chi N)_{ODT}$. Then, starting from such a configuration χ was turned off (to χ = 0) at time t = 0 and the evolution of the profiles was monitored. Figure 4 shows an

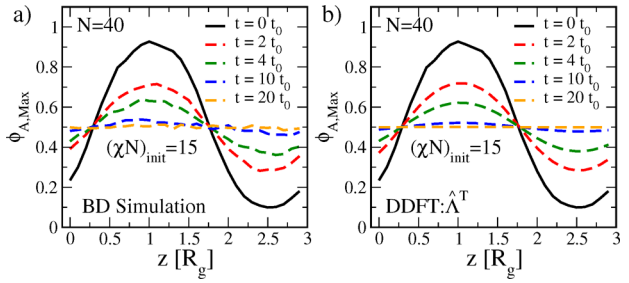

Figure 4. Evolution of density profile of A-monomers after a sudden change from $(\chi N)_{init}$ = 15 to χN = 0 at t = 0, according to (a) Brownian dynamics simulations and (b) DDFT calculations based on the relaxation time method, eq 24.

example of a series of resulting density profiles for A monomers at different times, as measured in a Brownian dynamics simulation run (Figure 4a)) and the corresponding results from DDFT calculations based on the relaxation time matrix (Figure 4b)). The DDFT calculations are in excellent agreement with the simulations.

To further quantify the comparison, we plot in Figure 5 the maximum value of the profile $\Phi_A(z)$ versus time for systems that were initially prepared at $(\chi N)_{init}$ = 15 (Figure 5a) and $(\chi N)_{init}$ = 20 (Figure 5b). Symbols show the simulation results, averaged over 10 independent runs, and lines show the results from different DDFT calculations. We find that DDFT calculations based on a chain coupling assumption (i.e., full chain dynamics, eq 5, or Debye dynamics $\hat{\Lambda}^{Debye}$, eq 6),

https://dx.doi.org/10.1021/acs.macromol.0c00130
Macromolecules 2020, 53, 3409−3423

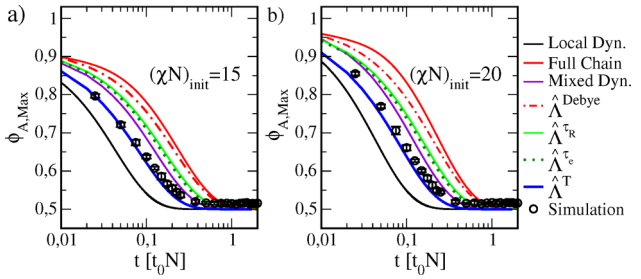

Figure 5. Relaxation of the maximum in the density profile of A-monomers for configurations that were initially equilibrated in an ordered phase at $(\chi N)_{init} = 15$ (a) and $(\chi N)_{init} = 20$ (b) after a sudden change to $\chi = 0$ at $t = 0$ for different DDFT schemes as indicated and compared to Brownian dynamics simulations at $N = 40$. The initial value $\phi_{A,Max}(t = 0)$ is the same in all calculations.

consistently underestimate the speed of the relaxation process. DDFT schemes with mobility functions $\hat{\Lambda}^{\tau}$ that were extracted assuming a single relaxation time $\tau(q)$ (i.e., eqs 21 and 22) perform better, but the dynamics is still too slow. The curves calculated with the "mixed coupling" scheme,[67] eq 11, are close by and also too slow. On the other hand, DDFT calculations based on a local coupling assumption overestimate the relaxation speed. In contrast, the predictions of DDFT calculations based on the relaxation time matrix, that is, on $\hat{\Lambda}^{\tau}$ (eq 24) are in excellent agreement with the simulation data.

4.3.2. Ordering Kinetics in a Symmetric Diblock Copolymer Melt. In our second example, we study the dynamics of structure formation in the block copolymer melt after a sudden quench from $\chi N = 0$ to some value $(\chi N) > (\chi N)_{ODT}$. An example for the time evolution of an A-density profile obtained from a Brownian dynamics simulation run and compared to DDFT calculations based on the relaxation time matrix is shown in Figure 6. In both cases, the initial density

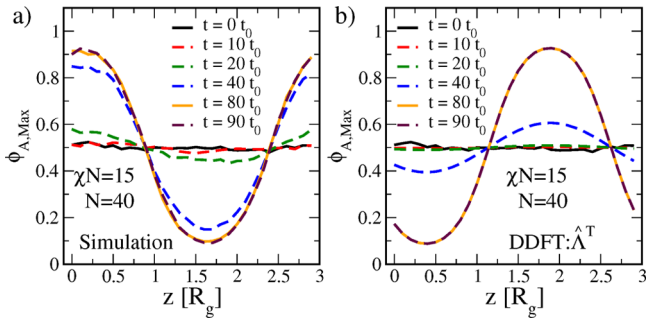

Figure 6. Evolution of density profile of A-monomers from an initially disordered conformation after the monomer interaction is suddenly raised from $\chi N = 0$ to $\chi N = 15$ at $t = 0$, according to (a) Brownian dynamics simulations and (b) DDFT calculations with mobility function based on eq 24.

profile is exactly the same, that is, small density fluctuations in the simulation profile were also transferred to the initial configuration in the DDFT calculation. Nevertheless, the agreement between simulations and DDFT calculations is less impressive than in the relaxation case, Figure 4. First, the location of the density maxima differs. This can be explained from the fact that the maxima emerge spontaneously at random positions in both cases. Second, the melt seems to order faster in the simulations than in the DDFT simulations. At the time $t = 40t_0$ after the quench, the amplitude of the oscillation in the A-density profile has almost saturated in the simulations, whereas it has only reached about one-fourth of the final value in the DDFT calculations.

On the other hand, looking at the simulations one notices that the ordering time also differs between different simulation runs. Figure 7 shows results for the maximum value of the A-

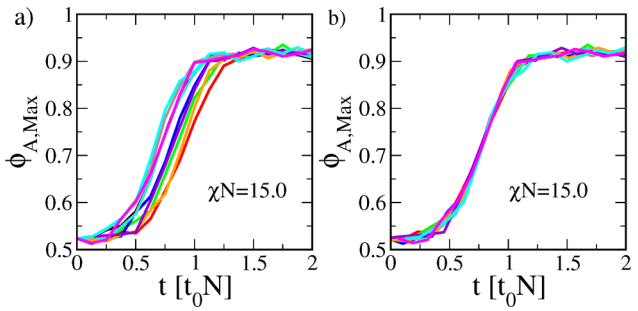

Figure 7. (a) Original and (b) aligned curves for the time evolution of the maximum in the spatial density of A-monomer after a sudden quench from $\chi N = 0$ to $\chi N = 15$ at $t = 0$ from 10 different Brownian dynamics simulation runs.

monomer density profile as a function of time for 10 different independent simulations, which all started from exactly the same initial configuration at $t = 0$. In every run, the lamellar ordering sets in at a different time (Figure 7 a). However, if one aligns the curves, that is, adds a time offset such that they coincide at half-maximum, their slopes fall largely on top of each other: The statistical spread of the onset of the ordering is much larger than the statistical noise after the ordering has set in. In the following, we therefore not only compare the kinetics of ordering on an absolute time scale but also the shape of the curves after they have been aligned.

Figure 8 shows the corresponding results for quenches to $\chi N = 15$ (Figure 8a,b) and to $\chi N = 20$ (Figure 8c,d), compared to a DDFT predictions from the different schemes discussed above. As reported in our earlier work[67] and consistent with our observations for the relaxation kinetics, Figure 5, DDFT calculations based on local dynamics (eq 4, black line) underestimate the ordering time, and DDFT calculations based on global chain dynamics (full chain dynamics (eq 5) or Debye dynamics (eq 6), red lines) overestimate it. Using DDFT mobilities that were extracted from bulk simulations assuming a single relaxation time, (eqs 21 or 22, green lines), the predicted ordering is faster than in the case of Debye dynamics but still too slow.

The best results are again obtained with the DDFT scheme $\hat{\Lambda}^{T}$ based on the relaxation time matrix, eq 24. The ordering in the DDFT calculations sets in later than in the simulations, but once started the dynamics of ordering is comparable. The delayed onset may be explained by the role of thermal fluctuations in initiating the ordering process. The DDFT calculations are purely deterministic and do not include fluctuations. Since the initial configurations are chosen identical to the simulated configurations, they include some noise, and that noise has the correct amplitude. As we have shown in earlier work,[67] the ordering would have been further delayed in all DDFT schemes if the initial noise level had been chosen lower. Nevertheless, adding noise to the initial configuration of a deterministic DDFT calculation is apparently not sufficient, if one wishes to faithfully reproduce the onset of ordering. To improve on this, one would have to

https://dx.doi.org/10.1021/acs.macromol.0c00130
Macromolecules 2020, 53, 3409−3423

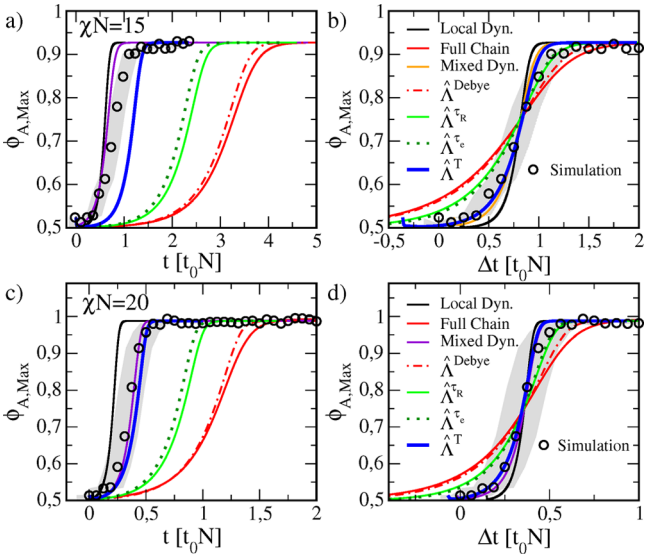

Figure 8. (a,c) Time evolution of the maximum density of A-monomers after a sudden quench from $\chi N = 0$ to when $\chi N = 15.0$ (a) and $\chi N = 20.0$ (c), according to Brownian dynamics simulations (symbols) and different DDFT schemes (lines) as indicated. The initial density profile in z-direction is the same in all calculations. Gray shades indicate spread of simulation curves (see Figure 7). (b,d) Same curves, aligned in time t.

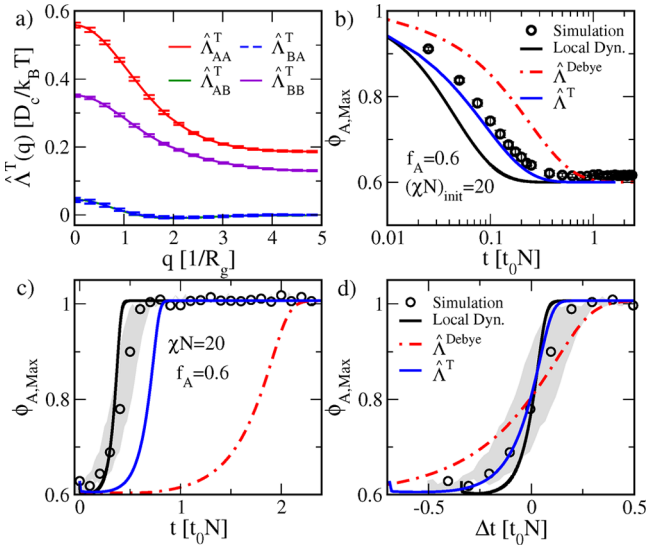

Figure 9. (a) Normalized mobility function $\hat{\Lambda}^T_{\alpha\beta}$ of asymmetric A/B diblock copolymers with block ratio 6:4 and length $N = 40$ obtained from simulations at $\chi N = 0$ with the relaxation time matrix approach (eq 24). (b–d) Corresponding time evolution of the maximum spatial density of A-monomers (b) after suddenly switching from $\chi N = 20$ to $\chi N = 0$ (c,d) and from $\chi N = 0$ to $\chi N = 20$ at $t = 0$ in absolute time (c) and aligned in time (d). Symbols correspond to Brownian Dynamics simulations with chain length $N = 40$, lines to results from DDFT calculations as indicated. Gray shades indicates spread of simulation curves from 10 independent configurations with identical starting configuration.

include thermal noise in the DDFT equations (see Section 5). Once initiated, the ordering proceeds in a deterministic manner and is very well captured by the DDFT calculations based on $\hat{\Lambda}^T$ (Figure 8b,d, blue line).

The results from "mixed dynamics" calculations (eq 11, cyan line) are also in very good agreement with the simulation data. However, it should be noted that this scheme has been postulated heuristically without any microscopic justification, and it has one free parameter (the parameter σ in eq 9) which has been optimized for this specific ordering situation in our earlier work.[67] In contrast, the mobility functions in the relaxation time scheme were determined from independent bulk simulations without any adjustable parameter. Also, from a practical point of view mixed dynamics calculations have the disadvantage that they require smaller time steps.

4.3.3. Asymmetric Diblock Copolymer Melt. So far, we have evaluated our different DDFT schemes by examining systems of symmetric diblock copolymer melts. To test whether the results depend on the symmetry of the system, we have repeated the analysis for a different A/B block fraction. The results are shown in Figure 9. We consider the same two situations as above: one where an initially lamellar morphology (set up in the ordered phase at $(\chi N)_{\text{init}} = 20$) relaxes into a homogeneous structure after turning χ off, and one where an initially disordered melt develops lamellar order after performing a quench into the ordered phase at $\chi N = 20$. The results are essentially the same as in the symmetric case: when using DDFT with "local dynamics", the dynamics is too fast; when using global chain dynamics (Debye dynamics), it is too slow. When using the relaxation time matrix approach, the onset of ordering is slightly delayed in the DDFT calculations compared to simulations but the actual ordering kinetics (the shape of the curves) is in very good agreement with the simulation data.

5. DISCUSSION AND SUMMARY

The purpose of the present work was to develop systematic bottom-up coarse-graining strategies for constructing nonlocal mobility functions $\hat{\Lambda}(\mathbf{q})$ in DDFT models for polymeric systems. The goal was to extract these mobility functions from trajectories of fine-grained, microscopic simulations. We have explored two physically motivated approaches.

The first was based on the Green–Kubo formalism. However, the Green–Kubo integrals were found to always vanish except at $\mathbf{q} = 0$ because the corresponding stationary current cannot exist at $\mathbf{q} \neq 0$. It was not even possible to identify a well-defined plateau in the running Green–Kubo integrals. Español et al.[104] have recently discussed such "plateau problems" and proposed an alternative approach to evaluating Green–Kubo transport coefficients. They suggested to analyze the late-time behavior of quantities $-(\frac{\mathrm{d}}{\mathrm{d}t}C(t))C^{-1}(t)$, where $C(t)$ is the time-dependent correlation function of the quantities of interest. In our case, the relevant correlation function is the single chain structure factor, $\underline{\underline{g}}(\mathbf{q}, t)$. Inserting eq 17 yields $\underline{\underline{\hat{\Lambda}}}(\mathbf{q}) \propto -q^2(\partial_t \underline{\underline{g}}(\mathbf{q}, t))\underline{\underline{g}}^{-1}(\mathbf{q}, t)\underline{\underline{g}}(\mathbf{q}, 0)$. Since the long-time behavior of $\underline{\underline{g}}(\mathbf{q}, t)$ is dominated by the diffusive behavior of whole chains, one has $\underline{\underline{g}}(\mathbf{q}, t) \propto \exp(-D_c q^2 t)$ at $t \to \infty$ and hence gets $\underline{\underline{\Lambda}}(\mathbf{q}) \propto D_c \underline{\underline{g}}(\mathbf{q}, 0)$, which corresponds to Debye dynamics. Thus, the resulting DDFT model is a "chain coupling" model where chains move as a whole.

In practice, however, we are interested in local ordering processes with characteristic time scales that are typically smaller than the diffusive time. Therefore, we have explored a second scheme, where a characteristic relaxation time matrix is

https://dx.doi.org/10.1021/acs.macromol.0c00130
Macromolecules 2020, 53, 3409–3423

first determined independently for each **q**-vector from fine-grained simulations, and this is then used to derive a **q**-dependent mobility matrix. As one can see from Figures 1 and 3, the resulting mobility functions are intermediate between "chain coupling dynamics" (chains move as a whole) and "local coupling dynamics" (monomers move independently). We have tested the approach by examining two kinetic processes in block copolymer melts: The process of disordering from an initially lamellar phase and the process of ordering after a quench into the lamellar phase. Comparing the DDFT calculations with the simulation results, we conclude that our new scheme is capable of describing the ordering/disordering kinetics at a quantitative level. Although we applied our model to study the order/disorder kinetics of lamellar structures only, the method can be applied to other morphologies as well (e.g., spheres, cylinders, and so forth).

We should note that although the kinetics of ordering and disordering are well-captured by the DDFT model, the onset of ordering is later than it should be, compared to simulations. We attribute this to the effect of thermal fluctuations, which are omitted in our DDFT calculations. They could be included by adding thermal noise to the density currents,[67] that is, replace eq 2 by

$$\partial_t \rho_\alpha = \nabla_r \left\{ \sum_\beta \int \mathrm{d}\mathbf{r}'\ \Lambda_{\alpha\beta}(\mathbf{r}, \mathbf{r}') \nabla_r \mu_\beta + \mathbf{j}_\alpha \right\} \tag{38}$$

where the stochastic current $\mathbf{j}_\zeta(\mathbf{r}, t)$ is to a Gaussian random vector field with zero mean ($\langle \mathbf{j}_\zeta(\mathbf{r}, t) \rangle = 0$) and correlations according to the fluctuation−dissipation theorem $\langle j_{I\alpha}(\mathbf{r},t)\, j_{J\beta}(\mathbf{r}',t') \rangle = 2k_\mathrm{B}T\delta(t-t')\, \hat{\Lambda}_{\alpha\beta}(\mathbf{r},\mathbf{r}')\, \delta_{IJ}$ (I, J are Cartesian coordinates).

It is worth recapitulating some of the approximations and assumptions that are entering our coarse-graining scheme.

First, we have assumed that the dynamics of inhomogeneous polymer systems can be described by an effective Markovian model. To account for the multitude of different relaxation times in polymer systems, we have treated the mobility as an adjustable **q**-dependent function; however, explicit memory effects were neglected. Wang et al.[66] have recently devised a dynamic RPA theory for polymer systems with a frequency dependent Onsager coefficient and showed that it successfully describes the decay of composition fluctuations in diblock copolymer melts (similar to Figure 4 here) and the onset of spinodal decomposition in homopolymer mixtures. Their Ansatz can easily be generalized to a dynamic SCF theory with a time-dependent memory kernel. It has the advantage that it includes memory explicitly, and does not require ad hoc adjustments of "effective" mobility functions. On the other hand, effective Markovian models are computationally more efficient in many cases.

Second, in eq 2 the mobility matrix describing the time evolution of density fluctuations should really be derived from the collective density correlations. Here, we have replaced them by a sum over intrachain density correlations in the spirit of a mean-field theory. Recently, Ghasimakbari and Morse[118] have used the collective structure factor to analyze the effective **q**-dependent diffusive relaxation of compositional fluctuations in symmetric diblock copolymer melts. They fitted the decay of the dynamic collective structure factor by a single exponential. Their results in the regime $(\chi N) < 10.5$ are comparable to ours in Figure 2.

Third, when deriving our final expression for $\underline{\Lambda}(\mathbf{q})$ in eq 16, we have linearized the free energy density functional and thus assumed that density variations are small. We determine the mobility function $\hat{\Lambda}(\mathbf{q})$ from simulations of a homogeneous bulk melt at $\chi N = 0$ but then use them in DDFT calculations for inhomogeneous, ordered systems. This is partly motivated by the finding that $\hat{\Lambda}(\mathbf{q})$ hardly depends on χ in the disordered regime of a block copolymer melt. Nevertheless, at high χ and/or in strongly inhomogeneous systems corrections must probably be applied.

We have formulated our approach for diblock copolymer melts, but it can easily be generalized to mixtures. Starting from eq 2, one can simply replace the mobility function $\Lambda_{\alpha\beta} \approx \Lambda^{(s)}_{\alpha\beta}\, \rho_0/N$ by a sum over chain mobilities, that is

$$\Lambda_{\alpha\beta}(\mathbf{r}, \mathbf{r}') = \sum_\gamma \frac{1}{N_\gamma} \bar{\rho}^{(\gamma)}(\mathbf{r}, \mathbf{r}') \Lambda^{(s,\gamma)}_{\alpha\beta}(\mathbf{r}, \mathbf{r}') \tag{39}$$

where the sum γ runs over chain types, N_γ is the length of chains of type γ, $\bar{\rho}^{(\gamma)}(\mathbf{r},\mathbf{r}')$ is the locally averaged density of monomers from chains of type γ (hence $\bar{\rho}^{\gamma}/N_\gamma$ is a chain density), and $\Lambda^{(s,\gamma)}_{\alpha\beta}$ is the corresponding single chain mobility function. Note that the prescription for determining the local average $\bar{\rho}^{(\gamma)}(\mathbf{r},\mathbf{r}')$ must be symmetric with respect to $\mathbf{r}$ and $\mathbf{r}'$ (e.g., $\bar{\rho}^{(\gamma)}(\mathbf{r}, \mathbf{r}') = \rho^{(\gamma)}\left(\frac{\mathbf{r}+\mathbf{r}'}{2}\right)$).

In mixtures, the diffusion of chains of different type adds another slow time scale to the dynamics of the system. In our previous work,[67] we have compared the dynamics of interdiffusion at A/B homopolymer interfaces from different DDFT calculations with simulations. We found that the results obtained with local and nonlocal DDFT coupling schemes were very similar, and all in very good agreement with the simulations. We conclude that studies of homopolymer interdiffusion do not seem to be a very sensitive test of the quality of a DDFT model, and therefore expect that the new schemes proposed here will also perform well.

Our bottom-up approach for constructing mobility matrices has been tested for Rouse chains but it is not restricted to that. It only requires as input the single chain dynamic structure factors from simulations of the target microscopic systems. In future work, we plan to study polymer mixtures and melts in other dynamical regimes, for example, entangled melts, or systems where hydrodynamics are important.

The DDFT theory relies on the assumption that the polymer system under consideration is only weakly disturbed from equilibrium. It assumes that the polymer conformations are close to local equilibrium at all times and that the dynamic process under consideration is still suitably described in terms of a free energy landscape picture. Therefore, it cannot be applied in situations far from equilibrium where the distribution of polymer conformations is distorted, such as, for example, polymers under shear at high Weissenberg numbers which are stretched out. Studying such systems with DDFT models requires novel approaches where not only the mobility functions but also the density functionals themselves have to be reconsidered.[119,120] However, DDFT theories that were constructed as proposed in the present paper can be used to study ordering processes and spontaneous self-assembly in inhomogeneous polymer mixtures and thus to evaluate the role of processing and pathways for the final structures.

https://dx.doi.org/10.1021/acs.macromol.0c00130
Macromolecules 2020, 53, 3409−3423

A. EVALUATION OF THE GREEN–KUBO INTEGRAL

In this appendix, we discuss the results from the evaluation of the integral (eq 13). In the spirit of mean-field theory, we will assume that the mobility can be derived from a single chain mobility, $\Lambda = \frac{\rho_0}{N}\Lambda^{(s)}$, which is derived from the current–current correlations of a single chain, that is, the quantity

$$\mathbf{I}_{\alpha\beta}(\mathbf{q}, t) = \sum_{k,j=1}^{N} e^{i\mathbf{q}\cdot(\mathbf{R}_k(t)-\mathbf{R}_j(0))}\dot{\mathrm{R}}_k(t)\dot{\mathrm{R}}_j(0)\gamma_k^{(\alpha)}\gamma_j^{(\beta)} \tag{40}$$

If interchain correlations can be neglected, one has $\langle \mathbf{j}_\alpha(\mathbf{q}, t)\, \mathbf{j}_\beta(-\mathbf{q}, t)\rangle = n_c \mathbf{I}_{\alpha\beta}(\mathbf{q}, t)$, where $n_c = V\frac{\rho_0}{N}$ is the number of polymers in the system and hence

$$\Lambda_{\alpha\beta}^{(s),\mathrm{GK}}(\mathbf{q}) = \frac{1}{k_B T}\int_0^\infty \mathrm{d}t\ \mathbf{I}_{\alpha\beta}(\mathbf{q}, t)\colon \hat{\mathbf{q}}\hat{\mathbf{q}} \tag{41}$$

The full chain mobility (all monomers) is given by the sum $\Lambda^{(s)}(\mathbf{q}) = \sum_{\alpha\beta}\Lambda_{\alpha\beta}^{(s)}(\mathbf{q})$.

We first discuss the full chain mobility at $\mathbf{q} = 0$. Equation 40 then reduces to $\mathbf{I}(0, t) = \sum_{\alpha\beta}\mathbf{I}_{\alpha\beta}(0, t) = \sum_{kj}\langle \dot{\mathrm{R}}_k(t)\dot{\mathrm{R}}_j(0)\rangle$. After evaluating the average of $\hat{\mathbf{q}}\hat{\mathbf{q}}$ with respect to all possible directions $\hat{\mathbf{q}}$, we recover the well-known relation between the chain mobility and the velocity autocorrelation function of the center of mass of the chain ($\mathbf{V}(t) = \frac{1}{N}\sum_k \dot{\mathrm{R}}_k(t)$):

$$\Lambda^{(s),\mathrm{GK}}(0) = \frac{N^2}{3k_B T}\int_0^\infty \mathrm{d}t\langle \mathbf{V}(t)\mathbf{V}(0)\rangle = \frac{D_c N^2}{k_B T} \tag{42}$$

Here D_c is the diffusion constant of the whole chain, and the factor N^2 accounts for the fact that $\Lambda^{(s)}$ describes the response of monomer current (scaling with the number N of monomers) to a thermodynamic force acting on monomers (i.e., the total force again scales with N).

For $\mathbf{q} \neq 0$ and $t > 0$, $\mathbf{I}_{\alpha\beta}(\mathbf{q}, t)$ can be derived from the single chain dynamic structure factor, defined as[63]

$$g_{\alpha\beta}(\mathbf{q}, t) = \frac{1}{N}\left\langle \sum_{k,j=1}^{N} e^{i\mathbf{q}\cdot(\mathbf{R}_k(t)-\mathbf{R}_j(0))}\gamma_k^{(\alpha)}\gamma_j^{(\beta)}\right\rangle \tag{43}$$

by taking the second derivative with respect to t

$$\mathbf{I}_{\alpha\beta}(\mathbf{q}, t)\colon \mathbf{qq} = -N\frac{\mathrm{d}^2}{\mathrm{d}t^2}g_{\alpha\beta}(\mathbf{q}, t) \tag{44}$$

Putting everything together, we finally obtain the following Green–Kubo relation between the mobility function and the single chain dynamic structure factor

$$\Lambda_{\alpha\beta}^{(s),\mathrm{GK}}(q) = \frac{N}{k_B T}\left(\frac{1}{q^2}\lim_{t\to 0}\left[\frac{\mathrm{d}}{\mathrm{d}t}g_{\alpha\beta}(q, t)\right] + \lim_{\epsilon\to 0}\int_0^\epsilon \mathrm{d}t\ \mathbf{I}_{\alpha\beta}(\mathbf{q})\colon \hat{\mathbf{q}}\hat{\mathbf{q}}\right) \tag{45}$$

This quantity can be measured in microscopic simulations. The second term in eq 46 has to be added explicitly if the microscopic model evolves according to overdamped Brownian dynamics, to account for the contribution of the delta-correlated stochastic white noise at $t = 0$ to eq 13.

Figure 10 shows simulation results for single chains in a homogeneous melt from Brownian dynamics and inertial dynamics simulations (see Section 4.1.1 for a detailed description of the simulation models). Figure 10a,b shows the results for $g(\mathbf{q}, t)$ for $qR_g = 1$ (a) and $qR_g = 4$ (b) and

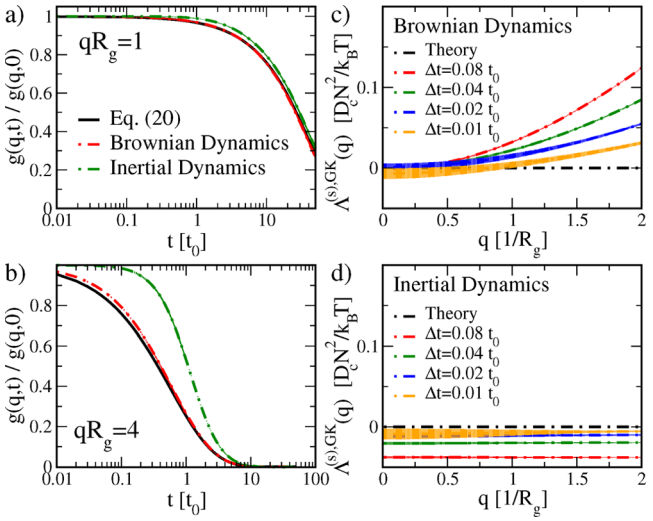

Figure 10. (Left) Normalized single chain dynamic structure factor of homopolymers with length $N = 40$ in a homopolymer melt, as obtained from Brownian dynamics (red) and inertial dynamics (green) simulations at $qR_g = 1.0$ (a) and $qR_g = 4.0$ (b). Black line shows the analytical prediction of eq 47. (Right) Normalized mobility function obtained via the Green–Kubo relation (eq 46) from Brownian dynamics (c) and inertial dynamics (d) simulations. The derivatives of $g(q, t)$ were taken numerically using a forward difference scheme with different values of Δt as indicated. The units t_0 and R_g are simulation units (see text).

compares them with an analytic result for ideal free Rouse chains,[63] which is exact in the limit $N \to \infty$

$$g(q, t) = \frac{1}{N}\sum_{ij}\exp\left[-q^2 D_c t - \frac{|i-j|(qR_g)^2}{N} - \frac{4(qR_g)^2}{\pi^2}\times\sum_{p=1}^{N}\frac{1}{p^2}\cos\left(\frac{p\pi i}{N}\right)\cos\left(\frac{p\pi j}{N}\right)\left\{1-\exp\left(-\frac{D_c t p^2\pi^2}{2R_g^2}\right)\right\}\right] \tag{46}$$

Here, the index p represents the pth Rouse mode, and the indices i, j represent the ith and jth beads on the polymer chain. The agreement with the Brownian dynamics simulaton data is very good. Figure 10 c,d) shows the corresponding Green–Kubo mobility functions. Somewhat disappointingly, they are found to be zero within the statistical and systematic error. Deviations from zero can be traced back to discretization artifacts when taking the derivative $\frac{\mathrm{d}}{\mathrm{d}t}g(q, t)$ numerically.

In the case of overdamped Rouse homopolymers, we can evaluate eq 46 exactly using the relation[63]

$$\frac{\mathrm{d}}{\mathrm{d}t}\ln g(q, t) = -\frac{1}{g(q, 0)}\frac{k_B T}{N}\sum_{kj}\langle \mathbf{H}_{kj}\exp(i\mathbf{q}\cdot(\mathbf{R}_k - \mathbf{R}_j))\rangle\colon \mathbf{qq} \tag{47}$$

with the Rouse mobility matrix $\mathbf{H}_{kj} = D_0\mathbf{1}\delta_{kj}$. The first term in eq 46 yields $\frac{1}{q^2}\frac{\mathrm{d}}{\mathrm{d}t}g(q, t)|_{t\to 0} = -D_0 N k_B T$. The noise term contributes with $2k_B T D_0 N\int_0^\epsilon \mathrm{d}t\ \delta(t) = D_0 N k_B T$. Since these two terms cancel, the resulting Green–Kubo mobility is zero, as suggested by the simulations.

https://dx.doi.org/10.1021/acs.macromol.0c00130
Macromolecules 2020, 53, 3409–3423

AUTHOR INFORMATION

Corresponding Author

Friederike Schmid − *Institut für Physik, Johannes Gutenberg Universität Mainz, 55128 Mainz, Germany;* orcid.org/0000-0002-5536-6718; Email: schmidfr@uni-mainz.de

Authors

Sriteja Mantha − *Institut für Physik, Johannes Gutenberg Universität Mainz, 55128 Mainz, Germany;* orcid.org/0000-0001-7813-0903

Shuanhu Qi − *Key Laboratory of Bio-inspired Smart Interfacial Science and Technology of Ministry of Education, School of Chemistry, Beihang University, Beijing 100191, China;* orcid.org/0000-0002-4260-4641

Complete contact information is available at: https://pubs.acs.org/10.1021/acs.macromol.0c00130

Notes

The authors declare no competing financial interest.

ACKNOWLEDGMENTS

We thank Marcus Müller for a critical reading of the manuscript and many useful comments. This research was supported by the German Science Foundation (DFG) via SFB TRR 146 (Grant 233630050, project C1). S.Q. acknowledges research support from the National Natural Science Foundation of China under Grant NSFC-21873010. The simulations were carried out on the high-performance computing center MOGON at JGU Mainz.

REFERENCES

(1) Hong, K. M.; Noolandi, J. Theory of Inhomogeneous Multicomponent Polymer Systems. *Macromolecules* **1981**, *14*, 727−736.

(2) Schacher, F. H.; Rupar, P. A.; Manners, I. Functional Block Copolymers: Nanostructured Materials with Emerging Applications. *Angew. Chem., Int. Ed.* **2012**, *51*, 7898−7921.

(3) Lynd, N. A.; Oyerokun, F. T.; O'Donoghue, D. L.; Handlin, D. L.; Fredrickson, G. H. Design of Soft and Strong Thermoplastic Elastomers Based on Nonlinear Block Copolymer Architectures Using Self-Consistent-Field Theory. *Macromolecules* **2010**, *43*, 3479−3486.

(4) Liechty, W. B.; Kryscio, D. R.; Slaughter, B. V.; Peppas, N. A. Polymers for Drug Delivery Systems. *Annu. Rev. Chem. Biomol. Eng.* **2010**, *1*, 149−173.

(5) Galizia, M.; Chi, W. S.; Smith, Z. P.; Merkel, T. C.; Baker, R. W.; Freeman, B. D. 50th Anniversary Perspective: Polymers and Mixed Matrix Membranes for Gas and Vapor Separation: A Review and Prospective Opportunities. *Macromolecules* **2017**, *50*, 7809−7843.

(6) Fane, A. G.; Wang, R.; Hu, M. X. Synthetic Membranes for Water Purification: Status and Future. *Angew. Chem., Int. Ed.* **2015**, *54*, 3368−3386.

(7) Peng, H.; Sun, X.; Weng, W.; Fang, X. In *Polymer Materials for Energy and Electronic Applications*; Peng, H., Sun, X., Weng, W., Fang, X., Eds.; Academic Press, 2017; pp 151 − 196.

(8) Peng, H.; Sun, X.; Weng, W.; Fang, X. In *Polymer Materials for Energy and Electronic Applications*; Peng, H., Sun, X., Weng, W., Fang, X., Eds.; Academic Press, 2017; pp 197 − 242.

(9) Black, C. T. Polymer Self-Assembly as a Novel Extension to Optical Lithography. *ACS Nano* **2007**, *1*, 147−150.

(10) Bates, C. M.; Bates, F. S. 50th Anniversary Perspective: Block Polymers − Pure Potential. *Macromolecules* **2017**, *50*, 3−22.

(11) Polymeropoulos, G.; Zapsas, G.; Ntetsikas, K.; Bilalis, P.; Gnanou, Y.; Hadjichristidis, N. 50th Anniversary Perspective: Polymers with Complex Architectures. *Macromolecules* **2017**, *50*, 1253−1290.

(12) Knychała, P.; Timachova, K.; Banaszak, M.; Balsara, N. P. 50th Anniversary Perspective: Phase Behavior of Polymer Solutions and Blends. *Macromolecules* **2017**, *50*, 3051−3065.

(13) Chen, W.-L.; Cordero, R.; Tran, H.; Ober, C. K. 50th Anniversary Perspective: Polymer Brushes: Novel Surfaces for Future Materials. *Macromolecules* **2017**, *50*, 4089−4113.

(14) Fredrickson, G. H.; Bates, F. S. Dynamics of Block Copolymers: Theory and Experiment. *Annu. Rev. Mater. Sci.* **1996**, *26*, 501−550.

(15) Tsarkova, L.; Horvat, A.; Krausch, G.; Zvelindovsky, A. V.; Sevink, G. J. A.; Magerle, R. Defect Evolution in Block Copolymer Thin Films via Temporal Phase Transitions. *Langmuir* **2006**, *22*, 8089−8095.

(16) Li, W.; Nealey, P. F.; de Pablo, J. J.; Müller, M. Defect Removal in the Course of Directed Self-Assembly is Facilitated in the Vicinity of the Order-Disorder Transition. *Phys. Rev. Lett.* **2014**, *113*, 168301.

(17) Li, W.; Müller, M. Defects in the Self-Assembly of Block Copolymers and Their Relevance for Directed Self-Assembly. *Annu. Rev. Chem. Biomol. Eng.* **2015**, *6*, 187−216.

(18) Hur, S.-M.; Khaira, G. S.; Ramirez-Hernandez, A.; Müller, M.; Nealey, P. F.; de Pablo, J. J. Simulation of Defect Reduction in Block Copolymer Thin Films by Solvent Annealing. *ACS Macro Lett.* **2015**, *4*, 11−15.

(19) Abate, A. A.; Vu, G. T.; Piqueras, C. M.; del Barrio, M. C.; Gomez, L. R.; Catalini, G.; Schmid, F.; Vega, D. A. Order-Order phase transitions induced by supercritical carbon dioxide in triblock copolymer thin films. *Macromolecules* **2019**, *52*, 7786−7797.

(20) Krishnamoorti, R.; Silva, A. S.; Modi, M. A.; Hammouda, B. Small-Angle Neutron Scattering Study of a Cylinder-to-Sphere Order-Order Transition in Block Copolymers. *Macromolecules* **2000**, *33*, 3803−3809.

(21) Bates, F. S.; Koppi, K. A.; Tirrell, M.; Almdal, K.; Mortensen, K. Influence of Shear on the Hexagonal-to-Disorder Transition in a Diblock Copolymer Melt. *Macromolecules* **1994**, *27*, 5934−5936.

(22) Sakurai, S.; Umeda, H.; Taie, K.; Nomura, S. Kinetics of Morphological Transition in Polystyrene-block-polybutadiene-block-polystyrene Triblock Copolymer < elt. *J. Chem. Phys.* **1996**, *105*, 8902−8908.

(23) Jeong, U.; Lee, H. H.; Yang, H.; Kim, J. K.; Okamoto, S.; Aida, S.; Sakurai, S. Kinetics and Mechanism of Morphological Transition from Lamella to Cylinder Microdomain in Polystyrene-block-poly(ethylene-co-but-1-ene)- block-polystyrene Triblock Copolymer. *Macromolecules* **2003**, *36*, 1685−1693.

(24) Sota, N.; Sakamoto, N.; Saijo, K.; Hashimoto, T. Phase Transition from Disordered Sphere to Hex-Cylinder via Transient Ordering into Bcc-Sphere in SIS Triblock Copolymer. *Macromolecules* **2003**, *36*, 4534−4543.

(25) Wang, C.-Y.; Lodge, T. P. Kinetics and Mechanisms for the Cylinder-to-Gyroid Transition in a Block Copolymer Solution. *Macromolecules* **2002**, *35*, 6997−7006.

(26) Hajduk, D. A.; Gruner, S. M.; Rangarajan, P.; Register, R. A.; Fetters, L. J.; Honeker, C.; Albalak, R. J.; Thomas, E. L. Observation of a Reversible Thermotropic Order-order Transition in a Diblock Copolymer. *Macromolecules* **1994**, *27*, 490−501.

(27) Schulz, M. F.; Bates, F. S.; Almdal, K.; Mortensen, K. Epitaxial Relationship for Hexagonal-to-Cubic Phase Transition in a Book Copolymer Mixture. *Phys. Rev. Lett.* **1994**, *73*, 86−89.

(28) Fiałkowski, M.; Hołyst, R. Quench-jump Sequence in Phase Separation in Polymer Blends. *J. Chem. Phys.* **2002**, *117*, 1886−1892.

(29) Coppée, S.; Gabriele, S.; Jonas, A. M.; Jestin, J.; Damman, P. Influence of Chain Interdiffusion Between Immiscible Polymers on Dewetting Dynamics. *Soft Matter* **2011**, *7*, 9951−9955.

(30) Xu, L.; Ankner, J. F.; Sukhishvili, S. A. Steric Effects in Ionic Pairing and Polyelectrolyte Interdiffusion within Multilayered Films: A Neutron Reflectometry Study. *Macromolecules* **2011**, *44*, 6518−6524.

(31) Klein, J. The Interdiffision of Polymers. *Science* **1990**, *250*, 640−646.

(32) Steiner, U.; Krausch, G.; Schatz, G.; Klein, J. Dynamics of mixing between partially miscible polymers. *Phys. Rev. Lett.* **1990**, *64*, 1119−1121.
(33) Guckenbiehl, B.; Stamm, M.; Springer, T. Interface properties of blends of incompatible polymers. *Phys. B* **1994**, *198*, 127−130.
(34) Scheffold, F.; Eiser, E.; Budkowski, A.; Steiner, U.; Klein, J.; Fetters, L. J. Surface Phase Behavior in Binary Polymer Mixtures. I. Miscibility, Phase Coexistence, and Interactions in Polyolefin Blends. *J. Chem. Phys.* **1996**, *104*, 8786−8794.
(35) Composto, R. J.; Walters, R. M.; Genzer, J. Application of Ion Scattering Techniques to Characterize Polymer Surfaces and Interfaces. *Mater. Sci. Eng., R* **2002**, *38*, 107−180.
(36) Lo, C.-T.; Narasimhan, B. A New Kinetic Model for Interdiffusion at Semicrystalline Polymer Interfaces. *Polymer* **2005**, *46*, 2266−2275.
(37) Schaefer, C.; Michels, J. J.; van der Schoot, P. Dynamic Surface Enrichment in Drying Thin-Film Binary Polymer Solutions. *Macromolecules* **2017**, *50*, 5914−5919.
(38) Fraaije, J. G. E. M. Dynamic Density Functional Theory for Microphase Separation Kinetics of Block Copolymer Melts. *J. Chem. Phys.* **1993**, *99*, 9202−9212.
(39) Kawasaki, K.; Sekimoto, K. Dynamical Theory of Polymer Melt Morphology. *Phys. A* **1987**, *143*, 349−413.
(40) Kawasaki, K.; Sekimoto, K. Morphology Dynamics of Block Copolymer Systems. *Phys. A* **1988**, *148*, 361−413.
(41) Fraaije, J. G. E. M.; van Vlimmeren, B. A. C.; Maurits, N. M.; Postma, M.; Evers, O. A.; Hoffmann, C.; Altevogt, P.; Goldbeck-Wood, G. The dynamic mean-field density functional method and its application to the mesoscopic dynamics of quenched block copolymer melts. *J. Chem. Phys.* **1997**, *106*, 4260−4269.
(42) Müller, M.; Schmid, F. In *Advanced Computer Simulation Approaches for Soft Matter Sciences II*; Holm, C., Kremer, K., Eds.; Springer Berlin Heidelberg: Berlin, Heidelberg, 2005; pp 1−58.
(43) Kawakatsu, T.; Doi, M.; Hasegawa, R. Dynamic Density Functional Approach to Phase Separation Dynamics of Polymer Systems. *Int. J. Mod. Phys. C* **1999**, *10*, 1531−1540.
(44) Binder, K. Dynamics of Phase Separation and Critical Phenomena in Polymer Mixtures. *Colloid Polym. Sci.* **1987**, *265*, 273−288.
(45) Schmid, F. Self-consistent Field Theories for Complex Fluids. *J. Phys.: Condens. Matter* **1998**, *10*, 8105−8138.
(46) Matsen, M. The Standard Gaussian Model for Block Copolymer Melts. *J. Phys.: Condens. Matter* **2002**, *14*, R21−R47.
(47) Fredrickson, G. H. *The Equilibrium Theory of Inhomogeneous Polymers*; Oxford University Press, 2006.
(48) He, X.; Schmid, F. Dynamics of Spontaneous Vesicle Formation in Dilute Solutions of Amphiphilic Diblock Copolymers. *Macromolecules* **2006**, *39*, 2654−2662.
(49) He, X.; Schmid, F. Spontaneous Formation of Complex Micelles from a Homogeneous Solution. *Phys. Rev. Lett.* **2008**, *100*, 137802.
(50) Wang, Y.; Li, X.; Tang, P.; Yang, Y. Dynamics and Order-disorder Transitions in Bidisperse Diblock Copolymer Blends. *Phys. B* **2011**, *406*, 1132−1138.
(51) Morita, H.; Kawakatsu, T.; Doi, M.; Yamaguchi, D.; Takenaka, M.; Hashimoto, T. Competition between Micro- and Macrophase Separations in a Binary Mixture of Block Copolymers. A Dynamic Density Functional Study. *Macromolecules* **2002**, *35*, 7473−7480.
(52) Morita, H.; Kawakatsu, T.; Doi, M. Dynamic Density Functional Study on the Structure of Thin Polymer Blend Films with a Free Surface. *Macromolecules* **2001**, *34*, 8777−8783.
(53) Reister, E.; Müller, M.; Binder, K. Spinodal Decomposition in a Binary Polymer Mixture: Dynamic Self-consistent-field Theory and Monte Carlo simulations. *Phys. Rev. E: Stat. Phys., Plasmas, Fluids, Relat. Interdiscip. Top.* **2001**, *64*, 041804.
(54) Yeung, C.; Shi, A.-C. Formation of Interfaces in Incompatible Polymer Blends:A Dynamical Mean Field Study. *Macromolecules* **1999**, *32*, 3637−3642.
(55) Qi, S.; Zhang, X.; Yan, D. External Potential Dynamic Studies on the Formation of Interface in Polydisperse Polymer Blends. *J. Chem. Phys.* **2010**, *132*, 064903.
(56) Reister, E.; Müller, M. Formation of Enrichment Layers in Thin Polymer Films: The Influence of Single Chain Dynamics. *J. Chem. Phys.* **2003**, *118*, 8476−8488.
(57) Maurits, N. M.; Zvelindovsky, A. V.; Sevink, G. J. A.; van Vlimmeren, B. A. C.; Fraaije, J. G. E. M. Hydrodynamic Effects in Three-dimensional Microphase Separation of Block Copolymers: Dynamic Mean-field Density Functional Approach. *J. Chem. Phys.* **1998**, *108*, 9150−9154.
(58) Honda, T.; Kawakatsu, T. Hydrodynamic Effects on the Disorder-to-order Transitions of Diblock Copolymer Melts. *J. Chem. Phys.* **2008**, *129*, 114904.
(59) Maurits, N. M.; Fraaije, J. G. E. M. Mesoscopic Dynamics of Copolymer Melts: From Density Dynamics to External Potential Dynamics Using Nonlocal Kinetic Coupling. *J. Chem. Phys.* **1997**, *107*, 5879−5889.
(60) Shima, T.; Kuni, H.; Okabe, Y.; Doi, M.; Yuan, X.-F.; Kawakatsu, T. Self-Consistent-Field Theory of Viscoelastic Behavior of Inhomogeneous Dense Polymer Systems. *Macromolecules* **2003**, *36*, 9199−9204.
(61) Weinan, E.; Weiqing, R.; Vanden-Eijnden, E. String method for the study of rare events. *Phys. Rev. B: Condens. Matter Mater. Phys.* **2002**, *66*, 052301.
(62) Ting, C. L.; Appelö, D.; Wang, Z.-G. Minimum Energy Path to Membrane Pore Formation and Rupture. *Phys. Rev. Lett.* **2011**, *106*, 168101.
(63) Doi, M.; Edwards, S. F. *The Theory of Polymer Dynamics*; Oxford University Press, 2013.
(64) Zwanzig, R. Memory Effects in Irreversible Thermodynamics. *Phys. Rev.* **1961**, *124*, 983−992.
(65) Mori, H. Transport, Collective Motion, and Brownian Motion. *Prog. Theor. Phys.* **1965**, *33*, 423−455.
(66) Wang, G.; Ren, Y.; Müller, M. Collective Short-Time Dynamics in Multicomponent Polymer Melts. *Macromolecules* **2019**, *52*, 7704−7720.
(67) Qi, S.; Schmid, F. Dynamic Density Functional Theories for Inhomogeneous Polymer Systems Compared to Brownian Dynamics Simulations. *Macromolecules* **2017**, *50*, 9831−9845.
(68) Han, Y.; Yu, H.; Du, H.; Jiang, W. Effect of Selective Solvent Addition Rate on the Pathways for Spontaneous Vesicle Formation of ABA Amphiphilic Triblock Copolymers. *J. Am. Chem. Soc.* **2010**, *132*, 1144−1150.
(69) Wu, M.; Wang, Y.; Han, Y.; Cui, J.; Jiang, W. A Facile Method for Preparation of Uniform Polymeric Vesicles With Tunable Size. *Nanoscale* **2018**, *10*, 14860.
(70) Ianiro, A.; Wu, H.; van Rijt, M. M. J.; Vena, M. P.; Keizer, A. D. A.; Esteves, A. C. C.; Tuinier, R.; Friedrich, H.; Sommerdijk, N. A. J. M.; Patterson, J. P. Liquid-liquid phase separation during amphiphilic self-assembly. *Nat. Chem.* **2019**, *11*, 320−328.
(71) Zeng, X.; Li, B.; Qiao, Q.; Zhu, L.; Lu, Z.-Y.; Huang, X. Elucidating Dominant Pathways of the Nano-particle Self-assembly Process. *Phys. Chem. Chem. Phys.* **2016**, *18*, 23494−23499.
(72) Chen, M.; Sun, M.; Wang, L.; Liu, X. Formation of Vesicles from Amphiphilic Random Copolymers in Solution: A Dissipative Particle Dynamics Simulation Study. *J. Dispersion Sci. Technol.* **2014**, *35*, 494−500.
(73) Xiao, M.; Xia, G.; Wang, R.; Xie, D. Controlling the Self-assembly Pathways of Amphiphilic Block Copolymers into Vesicles. *Soft Matter* **2012**, *8*, 7865−7874.
(74) Huang, J.; Wang, Y.; Qian, C. Simulation Study on the Formation of Vesicle and Influence of Solvent. *J. Chem. Phys.* **2009**, *131*, 234902.
(75) Sevink, G. J. A.; Zvelindovsky, A. V. Self-Assembly of Complex Vesicles. *Macromolecules* **2005**, *38*, 7502−7513.
(76) Zhang, L.; Sevink, A.; Schmid, F. Hybrid Lattice Boltzmann/Dynamic Self-Consistent Field Simulations of Microphase Separation

https://dx.doi.org/10.1021/acs.macromol.0c00130
Macromolecules 2020, 53, 3409−3423

and Vesicle Formation in Block Copolymer Systems. *Macromolecules* **2011**, *44*, 9434−9447.
(77) He, X.; Schmid, F. Using Prenucleation To Control Complex Copolymeric Veiscle Formation in Solution. *Macromolecules* **2006**, *39*, 8908−8910.
(78) Heuser, J.; Sevink, G. J. A.; Schmid, F. Self-Assembly of Polymeric Particles in Poiseuille Flow: A Hybrid Lattice Boltzmann/External Potential Dynamics Simulation Study. *Macromolecules* **2017**, *50*, 4474−4490.
(79) Lyubartsev, A. P.; Laaksonen, A. Calculation of Effective Interaction Potentials From Radial Distribution Functions: A Reverse Monte Carlo Approach. *Phys. Rev. E: Stat. Phys., Plasmas, Fluids, Relat. Interdiscip. Top.* **1995**, *52*, 3730−3737.
(80) Reith, D.; Pütz, M.; Müller-Plathe, F. Deriving Effective Mesoscale Potentials From Atomistic Simulations. *J. Comput. Chem.* **2003**, *24*, 1624−1636.
(81) Müller-Plathe, F. Coarse-Graining in Polymer Simulation: From the Atomistic to the Mesoscopic Scale and Back. *ChemPhysChem* **2002**, *3*, 754−769.
(82) Karimi-Varzaneh, H. A.; Müller-Plathe, F. In *Multiscale Molecular Methods in Applied Chemistry*; Kirchner, B., Vrabec, J., Eds.; Springer Berlin Heidelberg: Berlin, Heidelberg, 2012; pp 295−321.
(83) Gooneie, A.; Schuschnigg, S.; Holzer, C. A Review of Multiscale Computational Methods in Polymeric Materials. *Polymers* **2017**, *9*, 16.
(84) Deichmann, G.; van der Vegt, N. F. A. Bottom-up Approach to Represent Dynamic Properties in Coarse-grained Molecular Simulations. *J. Chem. Phys.* **2018**, *149*, 244114.
(85) Schnurr, B.; Gittes, F.; MacKintosh, F. C.; Schmidt, C. F. Determining Microscopic Viscoelasticity in Flexible and Semiflexible Polymer Networks from Thermal Fluctuations. *Macromolecules* **1997**, *30*, 7781−7792.
(86) Shin, H. K.; Kim, C.; Talkner, P.; Lee, E. K. Brownian Motion From Molecular Dynamics. *Chem. Phys.* **2010**, *375*, 316−326.
(87) Carof, A.; Vuilleumier, R.; Rotenberg, B. Two Algorithms to Compute Projected Correlation Functions in Molecular Dynamics Dimulations. *J. Chem. Phys.* **2014**, *140*, 124103.
(88) Li, Z.; Bian, X.; Li, X.; Karniadakis, G. E. Incorporation of Memory Effects in Coarse-grained Modeling via the Mori-Zwanzig Formalism. *J. Chem. Phys.* **2015**, *143*, 243128.
(89) Li, Z.; Lee, H. S.; Darve, E.; Karniadakis, G. E. Computing the Non-Markovian Coarse-grained Interactions Derived from the Mori-Zwanzig Formalism in Molecular Systems: Application to Polymer Melts. *J. Chem. Phys.* **2017**, *146*, 014104.
(90) Jung, G.; Hanke, M.; Schmid, F. Iterative Reconstruction of Memory Kernels. *J. Chem. Theory Comput.* **2017**, *13*, 2481−2488.
(91) Jung, G.; Hanke, M.; Schmid, F. Generalized Langevin dynamics: Construction and Numerical Integration of Non-Markovian Particle-based Models. *Soft Matter* **2018**, *14*, 9368−9382.
(92) Meyer, H.; Plagejcev, P.; Schilling, T. Non-Markovian Out-of-equilibrium Dynamics: A General Numerical Procedure to Construct Time-Dependent Memory Kernels for Coarse-grained Observables. *Europhys. Lett.* **2019**, *128*, 40001.
(93) Kubo, R.; Toda, M.; Hashitsume, N. *Statistical physics II*; Springer, 1985; Solid-State Sciences, Vol. *31*.
(94) Hansen, J. P.; McDonald, I. R. *Theory of Simple Liquids*; Academic Press, 2013.
(95) Kubo, R. The Fluctuation-dissipation Theorem. *Rep. Prog. Phys.* **1966**, *29*, 255−284.
(96) Evans, R. The Nature of the Liquid-vapour Interface and Other Topics in the Statistical Mechanics of Non-uniform, Classical Fluids. *Adv. Phys.* **1979**, *28*, 143−200.
(97) Mermin, N. D. Thermal Properties of the Inhomogeneous Electron Gas. *Phys. Rev.* **1965**, *137*, A1441−A1443.
(98) Hohenberg, P.; Kohn, W. Inhomogeneous Electron Gas. *Phys. Rev.* **1964**, *136*, B864−B871.
(99) Kohn, W.; Sham, L. J. Self-Consistent Equations Including Exchange and Correlation Effects. *Phys. Rev.* **1965**, *140*, A1133−A1138.
(100) Hohenberg, P. C.; Halperin, B. I. Theory of Dynamic Critical Phenomena. *Rev. Mod. Phys.* **1977**, *49*, 435−479.
(101) Rubinstein, M.; Colby, R. H. *Polymer physics*; Oxford University Press, 2008.
(102) Zwanzig, R. *Nonequilibrium Statistical Mechanics*; Oxford University Press, 2001.
(103) Kirkwood, J.; Buff, F.; Green, M. The Statistical Mechanical Theory of Transport Processes. III. The Coefficients of Shear and Bulk Viscosity of Liquids. *J. Chem. Phys.* **1949**, *17*, 988−994.
(104) Español, P.; de la Torre, J. A.; Duque-Zumajo, D. Solution to the plateau problem in the Green−Kubo formula. *Phys. Rev. E: Stat. Phys., Plasmas, Fluids, Relat. Interdiscip. Top.* **2019**, *99*, 022126.
(105) *MATLAB*, version 8.5 (R2015a); The MathWorks Inc.: Natick, MA, 2015.
(106) Edwards, S. F. The Statistical Mechanics of Polymers with Excluded Volume. *Proc. Phys. Soc., London* **1965**, *85*, 613−624.
(107) Laradji, M.; Guo, H.; Zuckermann, M. J. Off-lattice Monte Carlo Simulation of Polymer Brushes in Good Solvents. *Phys. Rev. E: Stat. Phys., Plasmas, Fluids, Relat. Interdiscip. Top.* **1994**, *49*, 3199−3206.
(108) Ganesan, V.; Pryamitsyn, V. Dynamical mean-field theory for inhomogeneous polymeric systems. *J. Chem. Phys.* **2003**, *118*, 4345−4348.
(109) Daoulas, K. C.; Müller, M. Single chain in mean field simulations: Quasi-instantaneous field approximation and quantitative comparison with Monte Carlo simulations. *J. Chem. Phys.* **2006**, *125*, 184904.
(110) Birdsall, C. K.; Fuss, D. Clouds-in-clouds, Clouds-in-cells Physics for Many-body Plasma Simulation. *J. Comput. Phys.* **1969**, *3*, 494−511.
(111) Detcheverry, F. A.; Kang, H.; Daoulas, K. C.; Müller, M.; Nealey, P. F.; dePablo, J. J. Monte Carlo Simulations of a Coarse Grain Model for Block Copolymers and Nanocomposites. *Macromolecules* **2008**, *41*, 4989−5001.
(112) Qi, S.; Klushin, L. I.; Skvortsov, A. M.; Polotsky, A. A.; Schmid, F. Stimuli-Responsive Brushes with Active Minority Components: Monte Carlo Study and Analytical Theory. *Macromolecules* **2015**, *48*, 3775−3787.
(113) Frenkel, D.; Smit, B. *Understanding Molecular Simulation: From Algorithms to Applications*; Academic Press, 2012.
(114) Brünger, A.; Brooks, C. L.; Karplus, M. Stochastic Boundary Conditions for Molecular Dynamics Simulations of ST2 Water. *Chem. Phys. Lett.* **1984**, *105*, 495−500.
(115) Schmid, F. *Handbook of Multiphase Polymer Systems*; Wiley-Blackwell, 2011; Chapter 3, pp 31−80.
(116) Gehlsen, M. D.; Almdal, K.; Bates, F. S. Order-disorder transition: diblock versus triblock copolymers. *Macromolecules* **1992**, *25*, 939−943.
(117) Rosedale, J. H.; Bates, F. S.; Almdal, K.; Mortensen, K.; Wignall, G. D. Order and Disorder in Symmetric Diblock Copolymer Melts. *Macromolecules* **1995**, *28*, 1429−1443.
(118) Ghasimakbari, T.; Morse, D. C. Dynamics and Viscoelasticity of Disordered Melts of Symmetric Diblock Copolymers. *Macromolecules* **2019**, *52*, 7762−7778.
(119) Müller, M.; Tang, J. Alignment of copolymer morphology by planar step elongation during spinodal self-assembly. *Phys. Rev. Lett.* **2015**, *115*, 228301.
(120) Chandran, S.; Baschnagel, J.; Cangialosi, D.; Fukao, K.; Glynos, E.; Janssen, L. M. C.; Muller, M.; Muthukumar, M.; Steiner, U.; Xu, J.; Napolitano, S.; Reiter, G. Processing Pathways Decide Polymer Properties at the Molecular Level. *Macromolecules* **2019**, *52*, 7146−7156.

https://dx.doi.org/10.1021/acs.macromol.0c00130
Macromolecules 2020, 53, 3409−3423